



LUND UNIVERSITY

Thick screens perforated with a periodic array of apertures with arbitrary cross-section

Widenberg, Björn; Poulsen, Sören; Karlsson, Anders

1999

[Link to publication](#)

Citation for published version (APA):

Widenberg, B., Poulsen, S., & Karlsson, A. (1999). *Thick screens perforated with a periodic array of apertures with arbitrary cross-section*. (Technical Report LUTEDX/(TEAT-7082)/1-30/(1999); Vol. TEAT-7082). [Publisher information missing].

Total number of authors:

3

General rights

Unless other specific re-use rights are stated the following general rights apply:

Copyright and moral rights for the publications made accessible in the public portal are retained by the authors and/or other copyright owners and it is a condition of accessing publications that users recognise and abide by the legal requirements associated with these rights.

- Users may download and print one copy of any publication from the public portal for the purpose of private study or research.
- You may not further distribute the material or use it for any profit-making activity or commercial gain
- You may freely distribute the URL identifying the publication in the public portal

Read more about Creative commons licenses: <https://creativecommons.org/licenses/>

Take down policy

If you believe that this document breaches copyright please contact us providing details, and we will remove access to the work immediately and investigate your claim.

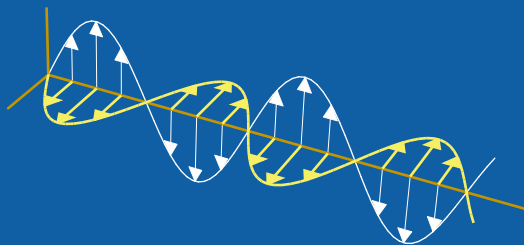
LUND UNIVERSITY

PO Box 117
221 00 Lund
+46 46-222 00 00

Thick screens perforated with a periodic array of apertures with arbitrary cross-section

Björn Widenberg, Sören Poulsen, and Anders Karlsson

Department of Electrosience
Electromagnetic Theory
Lund Institute of Technology
Sweden



Björn Widenberg, Sören Poulsen, and Anders Karlsson

Department of Electrosience

Electromagnetic Theory

Lund Institute of Technology

P.O. Box 118

SE-221 00 Lund

Sweden

Editor: Gerhard Kristensson

© Björn Widenberg, Sören Poulsen, and Anders Karlsson, Lund, June 8, 2001

Abstract

A plane wave impinges on a perfectly conducting thick screen perforated with a periodic array of apertures with arbitrary cross-section. The transmission and reflection coefficients are determined by a mode matching technique, earlier used by other authors for the case where the apertures have the geometry of a classical waveguide. The fields outside the screen are expanded in plane waves, while the fields inside the apertures are expanded in waveguide modes, obtained by the finite element method (FEM). Excellent agreement between computed and measured transmission is found for a thick screen at the X-band (8.2 – 12.4 GHz). Moreover, the present method and the spectral Galerkin method (which assumes that the thickness of the screen is zero) is compared for very thin screens, *e.g.*, for a frequency selective surface (FSS). Investigation of the thickness dependence is also done, and it is found that the bandwidth decreases when the thickness of the screen is increased. Finally two complex geometries, hexagonal and tripole apertures, are studied.

1 Introduction

In this paper we consider a perfectly conducting thick screen that is perforated with apertures with arbitrary cross-section. A plane wave impinges on the screen, and the reflection and transmission coefficients are computed by a mode matching technique where the tangential electric and magnetic fields are matched at the surfaces of the screen. In the present method, the fields outside the screen are expanded in tangential plane waves, *e.g.*, Floquet waves. Inside the apertures, the fields are expanded in waveguide modes that are computed by the finite element method (FEM).

An important application of thick screens is low observable radomes [13]. Here, the radome wall acts as a bandpass filter for electromagnetic waves such that only in-band waves are transmitted. The outband frequencies are reflected from the radome which reduces the radar cross-section (RCS) of the antenna that is shielded by the radome. The bandwidth of the thick screen can be increased by introducing patches that partly cover the aperture area [13].

In 1980, McPhedran, Derrick and Botten studied thick screens (they called them crossed gratings) with rectangular apertures [7]. However, their approach is limited to geometries where explicit expressions for the waveguide modes are available. In the PhD thesis of Roberts [8], annular apertures were considered (see also [10]). Then, in 1994, circular apertures were studied [11], and measurements in the far infrared were made. In this paper the geometry of the aperture is arbitrary. This is possible since we do not rely on explicit expressions for the waveguide modes. Instead we use the FEM to obtain appropriate waveguide modes. We do compare some of the numerical calculations with measurements performed at radar frequencies, *i.e.*, the X-band (8.2 – 12.4 GHz).

In the next section we recapitulate the mode matching technique developed by other authors [7, 8]. In Section 3 we discuss the computation of the waveguide modes and the FEM. The numerical results are presented in Section 4, where we

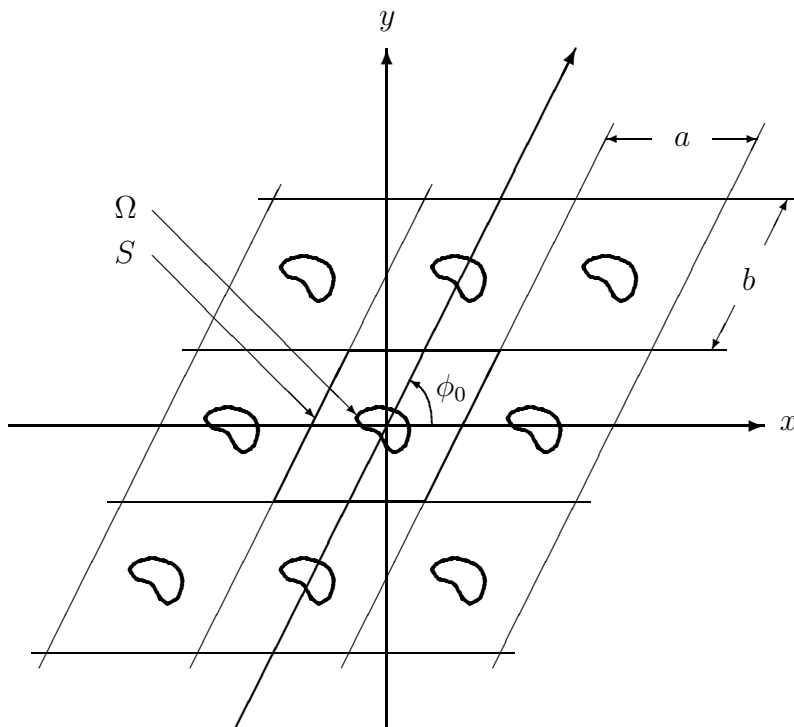


Figure 1: The geometry.

verify the method by measurements and the spectral Galerkin method [12]. Finally, computations for screens with hexagonal and tripole apertures are presented as examples of complex geometries.

2 Methods

The geometry of the screen is depicted in Figure 1. The z -axis is assumed to be orthogonal to the surface of the perfectly conducting screen. The upper surface of the screen coincide with $z = -h/2$, and the lower with $z = h/2$. The screen is perforated with apertures of arbitrary cross-section. These apertures are spaced periodically along the x -axis with period a . The other axis of periodicity makes an angle ϕ_0 with the x -axis and the apertures are spaced periodically along this second axis with period b , see Figure 1. Hence, the array of apertures is divided into identical cells. The cell at the origin is called the unit cell, and is denoted $S \in \mathbb{R}^2$. We define the area of the unit cell as $A_S := ab \sin \phi_0$. Moreover, the cross-section of the aperture at the unit cell is denoted $\Omega \in \mathbb{R}^2$, $\Omega \subset S$.

A plane wave, with wave vector $\mathbf{k}_0 := \hat{x}k_0 \sin \theta \cos \phi + \hat{y}k_0 \sin \theta \sin \phi + \hat{z}k_0 \cos \theta$, impinges on the screen. Here, θ and ϕ are the spherical angles of incidence, that is θ is the polar angle measured from the z -axis and ϕ is the azimuthal angle measured from the x -axis towards the y -axis. The wave number k_0 is given by $k_0 := \omega/c_0$, where $\omega := 2\pi f$, f is the frequency and c_0 is the speed of light in vacuum.

2.1 The Floquet waves

We introduce $\boldsymbol{\tau}_{mn} := \hat{x}\alpha_m + \hat{y}\beta_{mn}$, where the Floquet mode indices are given by [13]

$$\alpha_m := \frac{2\pi m}{a} + k_{0x}, \quad \beta_{mn} := \frac{2\pi n}{b \sin \phi_0} - \frac{2\pi m}{a} \cot \phi_0 + k_{0y}$$

Here, k_{0x} and k_{0y} is the x and y -component, respectively, of the wave vector $\mathbf{k}_0 = \hat{x}k_{0x} + \hat{y}k_{0y} + \hat{z}k_{0z}$. Thus $k_0^2 = k_{0x}^2 + k_{0y}^2 + k_{0z}^2 = \alpha_m^2 + \beta_{mn}^2 + \gamma_{mn}^2$. We define the scalar function

$$R_{mn}^\pm(\mathbf{r}) := \frac{1}{\sqrt{A_S}} e^{i(\boldsymbol{\tau}_{mn} \cdot \boldsymbol{\rho} \pm \gamma_{mn} z)}$$

where $\boldsymbol{\rho} := \hat{x}x + \hat{y}y$ and $\mathbf{r} := \boldsymbol{\rho} + \hat{z}z$. The principal square root branch is chosen such that the imaginary part of γ_{mn} is non-negative. We introduce the *Floquet waves* (denoted Rayleigh modes in [8])

$$\begin{aligned} \mathbf{R}_{1mn}^\pm(\mathbf{r}) &:= \mathbf{R}_{2mn}^\pm(\mathbf{r}) \times \hat{z} \\ \mathbf{R}_{2mn}^\pm(\mathbf{r}) &:= \hat{\tau}_{mn} R_{mn}^\pm(\mathbf{r}) \end{aligned}$$

where $\hat{\tau}_{mn} := \boldsymbol{\tau}_{mn}/|\boldsymbol{\tau}_{mn}|$. In fact, the Floquet waves are tangential plane waves. For $l = 1$ and $l = 2$, $\mathbf{R}_{lmn}^\pm(\mathbf{r})$ represents TE and TM polarized waves, respectively. Notice that the Floquet waves $\mathbf{R}_{lmn}^+(\mathbf{r})$ and $\mathbf{R}_{lmn}^-(\mathbf{r})$ propagate in negative and positive direction, respectively. Also, notice that $\mathbf{R}_{lmn}^+(\mathbf{r})$ and $\mathbf{R}_{lmn}^-(\mathbf{r})$ are equal for $z = 0$. Therefore we introduce $\mathbf{R}_{lmn}(\boldsymbol{\rho}) := \mathbf{R}_{lmn}^+(\boldsymbol{\rho}) = \mathbf{R}_{lmn}^-(\boldsymbol{\rho})$. The Floquet waves are orthonormal in the sense that

$$\int_S \mathbf{R}_{lmn}(\boldsymbol{\rho}) \cdot \mathbf{R}_{l'm'n'}^*(\boldsymbol{\rho}) \, dx \, dy = \delta_{ll'} \delta_{mm'} \delta_{nn'}$$

where $*$ denotes complex conjugate. Also, the Floquet waves fulfill the relation

$$\hat{z} \times (\nabla \times \mathbf{R}_{lmn}^\pm(\mathbf{r})) = \mp i \gamma_{mn} \mathbf{R}_{lmn}^\pm(\mathbf{r}) \quad (2.1)$$

2.2 Derivation of the normal component

The Floquet waves are tangential plane waves, *i.e.*, they do not contain the z -component of the expanded field. However, the z -component can be derived from the tangential component, that is, if \mathbf{E}_{xy} is a given tangential plane wave then the z -component, E_z , can be derived from \mathbf{E}_{xy} by a relation $\mathbf{E} = \overline{\overline{\mathbf{T}}} \cdot \mathbf{E}_{xy}$. In this section we derive the dyadic $\overline{\overline{\mathbf{T}}}$ which gives the total field from the tangential field.

First, we notice that for normal incidence, that is for $\theta = 0$, the z -component vanishes. Thus, without loss of generality we assume that $\theta > 0$. The electric field corresponding to a plane wave is denoted $\mathbf{E}(\mathbf{r})$. The wave propagates in the direction of the wave vector \mathbf{k} . We define

$$\mathbf{E}(\mathbf{r}) := \mathbf{P}(\boldsymbol{\xi}) e^{i\mathbf{k} \cdot \mathbf{r}}$$

where

$$\mathbf{P}(\xi) := \frac{\hat{z} \times \mathbf{k}}{|\hat{z} \times \mathbf{k}|} \cos \xi + \frac{\mathbf{k} \times (\hat{z} \times \mathbf{k})}{|\mathbf{k} \times (\hat{z} \times \mathbf{k})|} \sin \xi$$

is the polarisation of the plane wave. Here ξ is the polarisation angle, that is, $\xi = 0^\circ$ when the wave is TE-polarized, and $\xi = 90^\circ$ when the wave is TM-polarized. We decompose the electric field according to $\mathbf{E}(\mathbf{r}) = \mathbf{E}_{xy}(\mathbf{r}) + \hat{z}E_z(\mathbf{r})$. Here, the tangential field is easily obtained by applying the dyadic $\overline{\overline{\mathbf{I}}}_2 := \hat{x}\hat{x} + \hat{y}\hat{y}$, *i. e.*, $\mathbf{E}_{xy}(\mathbf{r}) = \overline{\overline{\mathbf{I}}}_2 \cdot \mathbf{P}(\xi)e^{i\mathbf{k}\cdot\mathbf{r}}$. Hence, we have

$$\hat{z}E_z(\mathbf{r}) = \mathbf{E}(\mathbf{r}) - \mathbf{E}_{xy}(\mathbf{r}) = (\overline{\overline{\mathbf{I}}} - \overline{\overline{\mathbf{I}}}_2) \cdot \mathbf{P}(\xi)e^{i\mathbf{k}\cdot\mathbf{r}} = \hat{z}\hat{z} \cdot \mathbf{P}(\xi)e^{i\mathbf{k}\cdot\mathbf{r}}$$

which can be simplified to

$$E_z(\mathbf{r}) = \frac{k_{xy}}{k} e^{i\mathbf{k}\cdot\mathbf{r}} \sin \xi$$

where $k_{xy} := (k_x^2 + k_y^2)^{1/2}$ is the length of the tangential wave vector $\mathbf{k}_{xy} := \overline{\overline{\mathbf{I}}}_2 \cdot \mathbf{k}$. On the other hand, by direct calculations it is found that

$$\mathbf{E}_{xy}(\mathbf{r}) = \left[\hat{z} \times \mathbf{k}_{xy} \cos \xi - \mathbf{k}_{xy} \frac{k_z}{k} \sin \xi \right] \frac{e^{i\mathbf{k}\cdot\mathbf{r}}}{k_{xy}}$$

Thus, we have

$$-\frac{\mathbf{k}_{xy}}{k_z} \cdot \mathbf{E}_{xy}(\mathbf{r}) = \frac{k_{xy}}{k} e^{i\mathbf{k}\cdot\mathbf{r}} \sin \xi = E_z(\mathbf{r})$$

and, hence, $\mathbf{E} = \overline{\overline{\mathbf{T}}} \cdot \mathbf{E}_{xy}$ where

$$\overline{\overline{\mathbf{T}}} := \overline{\overline{\mathbf{I}}} - \frac{\hat{z}\mathbf{k}_{xy}}{k_z} \quad (2.2)$$

For a wave propagating in the negative z -direction k_z in $\overline{\overline{\mathbf{T}}}$ changes sign to $-k_z$.

2.3 Expansion of the fields outside the structure

Above the screen, that is in the region $z > h/2$, the transverse part of the total electric field is denoted $\mathbf{E}_{xy}^+(\mathbf{r})$. On the other hand, the transversal part of the total field in the region $z < -h/2$ is denoted $\mathbf{E}_{xy}^-(\mathbf{r})$. These fields are expanded in Floquet waves as

$$\mathbf{E}_{xy} = \begin{cases} \mathbf{E}_{xy}^+(\mathbf{r}) = \sum_{lmn} E_{lmn}^+ \mathbf{R}_{lmn}^+(\mathbf{r}), & z > h/2 \\ \mathbf{E}_{xy}^-(\mathbf{r}) = \sum_{lmn} E_{lmn}^- \mathbf{R}_{lmn}^-(\mathbf{r}), & z < -h/2 \end{cases} \quad (2.3)$$

where the summation ranges over $\sum_{lmn} = \sum_{l=1}^2 \sum_{m=-\infty}^{\infty} \sum_{n=-\infty}^{\infty}$, and where $\mathbf{E}_{xy}^i(\mathbf{r})$ is the transversal part of the incident field, which is defined by

$$\mathbf{E}_{xy}^i(\mathbf{r}) := \sum_{lmn} E_{lmn}^i \mathbf{R}_{lmn}^+(\mathbf{r})$$

where the coefficients E_{lmn}^i are known. The corresponding expansions of the magnetic field are derived from the Faraday's law of induction,

$$\nabla \times \mathbf{E}(\mathbf{r}) = i\omega \mathbf{B}(\mathbf{r})$$

To see this we start with

$$\hat{z} \times \eta_0 \mathbf{H}_{xy}(\mathbf{r}) = \hat{z} \times \eta_0 \mathbf{H}(\mathbf{r}) = \frac{1}{ik_0} \hat{z} \times (\nabla \times \mathbf{E}(\mathbf{r}))$$

where the Faraday's law of induction and the relation $\mathbf{B} = \mu_0 \mathbf{H}$ was used. To proceed, we use the dyadic $\overline{\overline{T}}$, which gives the total field from the tangential one, see Eq. (2.2),

$$\hat{z} \times \eta_0 \mathbf{H}_{xy} = \frac{1}{ik_0} \hat{z} \times (\nabla \times \overline{\overline{T}} \cdot \mathbf{E}_{xy}) \quad (2.4)$$

In this context, $\overline{\overline{T}} = \overline{\overline{I}} \mp \hat{z} \tau_{mn} / \gamma_{mn}$, where the upper and lower sign corresponds to waves propagating in positive and negative z -direction, respectively. Thus we have

$$\begin{cases} \overline{\overline{T}} \cdot \mathbf{R}_{1mn}^\pm(\mathbf{r}) = \mathbf{R}_{1mn}^\pm(\mathbf{r}) \\ \overline{\overline{T}} \cdot \mathbf{R}_{2mn}^\pm(\mathbf{r}) = \mathbf{R}_{2mn}^\pm(\mathbf{r}) \mp \frac{\hat{z} \tau_{mn}}{\gamma_{mn}} \mathbf{R}_{mn}^\pm(\mathbf{r}) \end{cases}$$

Relation (2.1) now yields

$$\begin{cases} \hat{z} \times (\nabla \times \overline{\overline{T}} \cdot \mathbf{R}_{1mn}^\pm(\mathbf{r})) = \mp i \gamma_{mn} \mathbf{R}_{1mn}^\pm(\mathbf{r}) \\ \hat{z} \times (\nabla \times \overline{\overline{T}} \cdot \mathbf{R}_{2mn}^\pm(\mathbf{r})) = \mp \frac{ik_0^2}{\gamma_{mn}} \mathbf{R}_{2mn}^\pm(\mathbf{r}) \end{cases}$$

where we made use of the fact that

$$\hat{z} \times (\nabla \times (\mp \hat{z} \tau_{mn} \mathbf{R}_{mn}^\pm(\mathbf{r}) / \gamma_{mn})) = \pm i \tau_{mn}^2 \mathbf{R}_{2mn}^\pm(\mathbf{r}) / \gamma_{mn}$$

From the expansions (2.3), and from Eq. (2.4), we get

$$\eta_0 \hat{z} \times \mathbf{H}_{xy}(\mathbf{r}) = \begin{cases} \eta_0 \hat{z} \times \mathbf{H}_{xy}^+(\mathbf{r}) = - \sum_{lmn} Y_{lmn} E_{lmn}^+ \mathbf{R}_{lmn}^+(\mathbf{r}), & z > h/2 \\ \eta_0 \hat{z} \times \mathbf{H}_{xy}^i(\mathbf{r}) + \eta_0 \hat{z} \times \mathbf{H}_{xy}^-(\mathbf{r}) \\ \quad = \eta_0 \hat{z} \times \mathbf{H}_{xy}^i(\mathbf{r}) + \sum_{lmn} Y_{lmn} E_{lmn}^- \mathbf{R}_{lmn}^-(\mathbf{r}), & z < -h/2 \end{cases}$$

where $\eta_0 := (\mu_0 / \epsilon_0)^{1/2}$ is the wave impedance of free space and $Y_{lmn} := (\gamma_{mn} / k_0)^{3-2l}$. Moreover, we have

$$\eta_0 \hat{z} \times \mathbf{H}_{xy}^i(\mathbf{r}) = - \sum_{lmn} Y_{lmn} E_{lmn}^i \mathbf{R}_{lmn}^+(\mathbf{r})$$

2.4 Expansion of the field in the apertures

In the previous subsection the fields outside the structure were expanded in Floquet waves. Now, we consider the field inside the apertures. If the apertures have the geometry of a classical waveguide, the field is expanded in appropriate waveguide modes, and explicit expressions for the modes are then used. Several of the classic waveguide geometries have been considered in the literature, for instance, rectangular apertures [7], annular apertures [8–10] and circular apertures [11]. However, for a general cross-section of the apertures, explicit expressions for the waveguide modes are not available. Instead, we compute these modes with the FEM, see Section 3.

We assume that the media inside the waveguide is homogeneous and isotropic. The relative permittivity of the media is denoted $\epsilon(\omega)$, while the relative permeability is denoted $\mu(\omega)$. The wave number in the waveguide is denoted $k(\omega) = k_0(\mu(\omega)\epsilon(\omega))^{1/2}$ and $\eta(\omega) = (\mu(\omega)/\epsilon(\omega))^{1/2}$ is the relative wave impedance.

Moreover, we assume that $\mathbf{E}_p^T(\boldsymbol{\rho})$ is a complete set of modes defined on the cross-section of the aperture at the unit cell, *i.e.*, $\boldsymbol{\rho} \in \Omega$. For classical waveguide geometries these modes are given explicitly, but for general geometry of the apertures they are computed by the FEM as described in Section 3. The tangential electric field is expanded in the waveguide modes as ($\boldsymbol{\rho} \in \Omega$, $-h/2 \leq z \leq h/2$)

$$\mathbf{E}^T(\mathbf{r}) = \sum_{p \in \chi} [A_p \sin(k_{zp}z) + B_p \cos(k_{zp}z)] \mathbf{E}_p^T(\boldsymbol{\rho}) \quad (2.5)$$

where $p = (l, n)$ belongs to the index-set of the waveguide modes, χ , and where l and n are integers defining the type of the mode. Here, $l = 0$ represents the TEM mode, $l = 1$ a TE mode, and $l = 2$ a TM mode. When the apertures have the geometry of a classical waveguide, and the FEM is not used, it is convenient to let n be a multi-index, cf. [7–10]. From the expansion (2.5) the magnetic field is derived, see Section 3.1,

$$\eta_0 \eta(\omega) \hat{z} \times \mathbf{H}^T(\mathbf{r}) = \sum_{p \in \chi} \nu_p [A_p \cos(k_{zp}z) - B_p \sin(k_{zp}z)] \mathbf{E}_p^T(\boldsymbol{\rho}) \quad (2.6)$$

where $\nu_p = i(k_{zp}/k(\omega))^{l(5-3l)/2}$, $l = 0, 1, 2$.

2.5 Enforcing the boundary conditions

We have expressions for the electric and magnetic fields outside the structure and inside the apertures. We enforce the boundary conditions at the interfaces $z = \pm h/2$. The boundary conditions say that the tangential electric field is continuous over the entire interfaces, while the magnetic field is continuous over the apertures, that is

$$\begin{aligned} \mathbf{E}_{xy}(\boldsymbol{\rho} \pm \hat{z}h/2) &= \mathbf{E}^T(\boldsymbol{\rho} \pm \hat{z}h/2), & \boldsymbol{\rho} \in S \\ \hat{z} \times \mathbf{H}_{xy}(\boldsymbol{\rho} \pm \hat{z}h/2) &= \hat{z} \times \mathbf{H}^T(\boldsymbol{\rho} \pm \hat{z}h/2), & \boldsymbol{\rho} \in \Omega \end{aligned}$$

We introduce

$$\begin{aligned}
e_{lmn}^i &:= E_{lmn}^i e^{-i\gamma_{lmn}h/2} \\
e_{lmn}^\pm &:= E_{lmn}^\pm e^{i\gamma_{lmn}h/2} \\
a_p^E &:= A_p \sin(k_{zp}h/2) \\
b_p^E &:= B_p \cos(k_{zp}h/2) \\
a_p^H &:= A_p \cos(k_{zp}h/2) \\
b_p^H &:= B_p \sin(k_{zp}h/2)
\end{aligned}$$

Enforcing the continuity condition of the electric field at the interface $z = h/2$ yields

$$\sum_{lmn} e_{lmn}^+ \mathbf{R}_{lmn}(\boldsymbol{\rho}) = \begin{cases} \sum_p (a_p^E + b_p^E) \mathbf{E}_p^T(\boldsymbol{\rho}), & \boldsymbol{\rho} \in \Omega \\ \mathbf{0}, & \boldsymbol{\rho} \in \Omega^{PEC} = S \setminus \Omega \end{cases} \quad (2.7a)$$

while the condition at $z = -h/2$ yields

$$\sum_{lmn} (e_{lmn}^- + e_{lmn}^i) \mathbf{R}_{lmn}(\boldsymbol{\rho}) = \begin{cases} \sum_p (-a_p^E + b_p^E) \mathbf{E}_p^T(\boldsymbol{\rho}), & \boldsymbol{\rho} \in \Omega \\ \mathbf{0}, & \boldsymbol{\rho} \in \Omega^{PEC} \end{cases} \quad (2.7b)$$

Moreover, the continuity condition of the magnetic field at the apertures at $z = h/2$, implies

$$-\sum_{lmn} Y_{lmn} e_{lmn}^+ \mathbf{R}_{lmn}(\boldsymbol{\rho}) = \sum_p \nu_p (a_p^H - b_p^H) \mathbf{E}_p^T(\boldsymbol{\rho}), \quad \boldsymbol{\rho} \in \Omega \quad (2.7c)$$

while, at the interface $z = -h/2$, we get

$$\sum_{lmn} Y_{lmn} (e_{lmn}^- - e_{lmn}^i) \mathbf{R}_{lmn}(\boldsymbol{\rho}) = \sum_p \nu_p (a_p^H + b_p^H) \mathbf{E}_p^T(\boldsymbol{\rho}), \quad \boldsymbol{\rho} \in \Omega \quad (2.7d)$$

2.6 The linear system for the waveguide coefficients

To obtain a linear system of equations for the waveguide coefficients we eliminate the plane wave coefficients e_{lmn}^\pm . First, we multiply Eq. (2.7a) with $\mathbf{R}_{l'm'n'}^*(\boldsymbol{\rho})$ and integrate over the unit cell S . We get

$$e_{l'm'n'}^+ = \sum_p (a_p^E + b_p^E) \mathbf{E}_p^T * \mathbf{R}_{l'm'n'} \quad (2.8a)$$

where the orthogonal property of the Floquet waves was used and

$$\mathbf{E}_p^T * \mathbf{R}_{l'm'n'} := \int_S \mathbf{E}_p^T(\boldsymbol{\rho}) \cdot \mathbf{R}_{l'm'n'}^*(\boldsymbol{\rho}) \, dS.$$

Similarly, Eq. (2.7b) yields

$$e_{l'm'n'}^- + e_{l'm'n'}^i = \sum_p (-a_p^E + b_p^E) \mathbf{E}_p^T * \mathbf{R}_{l'm'n'} \quad (2.8b)$$

Furthermore, we multiply Eq. (2.7c) and Eq. (2.7d) with $\mathbf{E}_{p'}^T(\boldsymbol{\rho})$, and integrate over Ω ,

$$-\sum_{lmn} Y_{lmn} e_{lmn}^+ \mathbf{E}_{p'}^T * \mathbf{R}_{lmn}^* = \nu_{p'} (a_{p'}^H - b_{p'}^H) \quad (2.9a)$$

$$\sum_{lmn} Y_{lmn} (e_{lmn}^- - e_{lmn}^i) \mathbf{E}_{p'}^T * \mathbf{R}_{lmn}^* = \nu_{p'} (a_{p'}^H + b_{p'}^H) \quad (2.9b)$$

The coefficients e_{lmn}^\pm are eliminated by Eqs. (2.8a) and (2.8b),

$$\begin{aligned} \sum_p (a_p^E + b_p^E) I_p^{p'} + \nu_{p'} (a_{p'}^H - b_{p'}^H) &= 0 \\ \sum_p (-a_p^E + b_p^E) I_p^{p'} - \nu_{p'} (a_{p'}^H + b_{p'}^H) &= 2 \sum_{lmn} Y_{lmn} e_{lmn}^i \mathbf{E}_{p'}^T * \mathbf{R}_{lmn}^* \end{aligned}$$

where $I_p^{p'} := \sum_{l''m''n''} Y_{l''m''n''} \mathbf{E}_{p'}^T * \mathbf{R}_{l''m''n''}^* \mathbf{E}_p^T * \mathbf{R}_{l''m''n''}$. By adding and subtracting these equations we obtain

$$\begin{aligned} \sum_p a_p^E I_p^{p'} + \nu_{p'} a_{p'}^H &= - \sum_{lmn} Y_{lmn} e_{lmn}^i \mathbf{E}_{p'}^T * \mathbf{R}_{lmn}^* \\ \sum_p b_p^E I_p^{p'} - \nu_{p'} b_{p'}^H &= \sum_{lmn} Y_{lmn} e_{lmn}^i \mathbf{E}_{p'}^T * \mathbf{R}_{lmn}^* \end{aligned}$$

or

$$\sum_p A_p (\sin(k_{zp}h/2) I_p^{p'} + \nu_p \cos(k_{zp}h/2) \delta_{pp'}) = -J_{p'} \quad (2.10a)$$

$$\sum_p B_p (\cos(k_{zp}h/2) I_p^{p'} - \nu_p \sin(k_{zp}h/2) \delta_{pp'}) = J_{p'} \quad (2.10b)$$

where $J_{p'} := \sum_{lmn} Y_{lmn} e_{lmn}^i \mathbf{E}_{p'}^T * \mathbf{R}_{lmn}^*$. Hence, we obtain two non-coupled systems of equations for the waveguide coefficients A_p and B_p . The linear systems (2.10a) and (2.10b) are solved by inverting the matrices. Once the waveguide coefficients A_p and B_p are known, the plane wave coefficients e_{lmn}^\pm are easily obtained from Eqs. (2.8a) and (2.8b).

2.7 The scattering matrices

Since the incident field is given by an arbitrary Floquet wave (or a sum of Floquet waves), it is straightforward to define the reflection and transmission matrices [13] of the structure. These scattering matrices are used when the periodic structure is cascaded together with other structures, for instance dielectric layers or FSS:s, to form more general structures. The scattering matrices contain generalized reflection and transmission coefficients, so that a specific column in the matrix is valid for a specific incident Floquet wave, while a specific row corresponds to a specific scattered Floquet wave.

To this end it is necessary to pay special attention to the phase of the reflected and transmitted fields. If we define the coefficients of the incident field as

$$E_{lmn}^i = e^{i\gamma_{mn}h/2} \delta_{ll^i mm^i nn^i}$$

then the phase center of the incident field is located at $z = -h/2$, that is, the phase of the incident field is zero at the point $\mathbf{r} = -\hat{z}h/2$. The integers l^i , m^i , and n^i defines the specific Floquet wave that the incident field consists of. Thus, we have $e_{lmn}^i = \delta_{ll^i mm^i nn^i}$. We calculate the waveguide coefficients A_p and B_p for the specific incident field, and then the coefficients of the reflected field is given by Eq. (2.8b) as

$$e_{lmn}^- = -e_{lmn}^i + \sum_{p \in \chi} (-A_p \sin(k_{zp}h/2) + B_p \cos(k_{zp}h/2)) \mathbf{E}_p^T * \mathbf{R}_{lmn}$$

On the other hand, the reflected field is given by

$$\mathbf{E}_{xy}^-(\mathbf{r}) = \sum_{lmn} E_{lmn}^- \mathbf{R}_{lmn}^-(\mathbf{r}) = \sum_{lmn} \underbrace{E_{lmn}^- e^{i\gamma_{mn}h/2}}_{\text{Ref. coeff.}} \underbrace{e^{-i\gamma_{mn}h/2} \mathbf{R}_{lmn}^-(\mathbf{r})}_{\text{Correct phase center}}$$

where the phase center of $e^{-i\gamma_{mn}h/2} \mathbf{R}_{lmn}^-(\mathbf{r})$ is located at $z = -h/2$. Hence, the reflection coefficient, related to the interface $z = -h/2$, is given by $E_{lmn}^- e^{i\gamma_{mn}h/2}$, which equals e_{lmn}^- . Similarly, the plane wave coefficients of the transmitted field are given by Eq. (2.8a) as

$$e_{lmn}^+ = \sum_{p \in \chi} (A_p \sin(k_{zp}h/2) + B_p \cos(k_{zp}h/2)) \mathbf{E}_p^T * \mathbf{R}_{lmn}$$

The transmitted field is given by

$$\mathbf{E}_{xy}^+(\mathbf{r}) = \sum_{lmn} E_{lmn}^+ \mathbf{R}_{lmn}^+(\mathbf{r}) = \sum_{lmn} \underbrace{E_{lmn}^+ e^{i\gamma_{mn}h/2}}_{\text{Trans. coeff.}} \underbrace{e^{-i\gamma_{mn}h/2} \mathbf{R}_{lmn}^+(\mathbf{r})}_{\text{Correct phase center}}$$

where the phase center of $e^{-i\gamma_{mn}h/2} \mathbf{R}_{lmn}^+(\mathbf{r})$ is located at $z = h/2$. Thus, the transmission coefficient, related to the interface $z = h/2$, is defined as $E_{lmn}^+ e^{i\gamma_{mn}h/2}$, that is e_{lmn}^+ .

To describe how the scattering matrices are build up, we use the following pseudo code.

```
do col=1,size of scattering matrices
  define incident field from col
  define right hand side
  calculate  $A_p$  and  $B_p$ 
  do row=1,size of scattering matrices
    define  $l$ ,  $m$  and  $n$  from row
    reflection matrix(row,col)= $e_{lmn}^-$ 
    transmission matrix(row,col)= $e_{lmn}^+$ 
  end do
end do
```

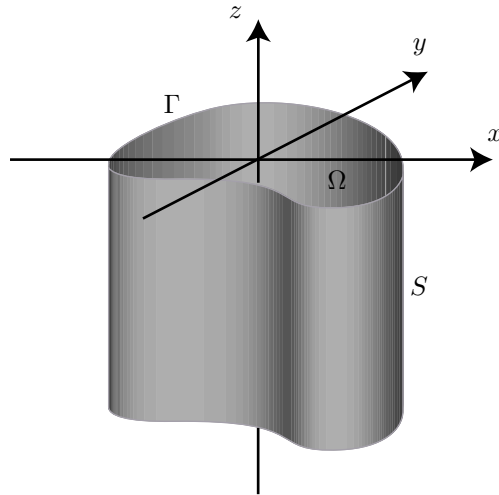


Figure 2: Geometry for a waveguide

3 Waveguide modes and FEM

According to the previous section the electromagnetic fields inside the apertures are expanded in waveguide modes. In this section we describe how the waveguide modes are obtained by solving a scalar eigenvalue problem by the FEM.

3.1 Waveguide theory

The geometry for a cylindric waveguide with arbitrary cross-section is depicted in Figure 2. The boundary surface is denoted S , the cross-section is denoted Ω and its cross-sectional contour is denoted Γ . Figure 3(a) shows a waveguide with a simply connected cross-section Ω , while Figure 3(b) shows a waveguide with a boundary contour Γ that consists of two non-connected parts. The outward normal of the waveguide, \hat{n} , is a function of x and y , but is independent of the variable z . The boundary surface is a perfect conductor and it is assumed that the waveguide is either empty or else filled with a homogeneous isotropic medium with electrical parameters $\epsilon(\omega)$ and $\mu(\omega)$. We further assume that there are no sources in the waveguide.

Standard waveguide theory gives that the z -dependence of all field vectors in the waveguide is given by $e^{\pm ik_z z}$, where k_z is the propagation constant and the $+$ ($-$) sign indicates propagation along the positive (negative) z -direction.

In the waveguide in Figure 3(a) two different modes, the transverse electric (TE) mode and the transverse magnetic (TM) mode, can exist. In the waveguide with an inner conductor, cf. Fig. 3(b), the transverse electromagnetic (TEM) mode can also exist, see [2]. Thus $H_z = 0$ for the TM modes, $E_z = 0$ for the TE modes, and both $H_z = 0$ and $E_z = 0$ for the TEM mode.

The field components for the TM modes are derived from the eigenvalue problem, see for example [4], given by Helmholtz's equation with a homogeneous Dirichlet

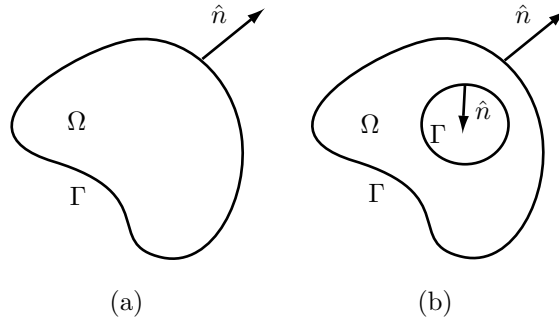


Figure 3: Waveguide cross-section

boundary condition,

$$\begin{cases} \nabla_T^2 v_{2n}(\boldsymbol{\rho}) + k_{t2n}^2 v_{2n}(\boldsymbol{\rho}) = 0, & \boldsymbol{\rho} \in \Omega, \\ v_{2n}(\boldsymbol{\rho}) = 0, & \boldsymbol{\rho} \in \Gamma, \end{cases} \quad (3.1)$$

where $k_{t2n}^2 = k^2 - k_{z2n}^2$ and ∇_T^2 is the transverse part of the ∇^2 -operator, *i.e.*, $\nabla_T^2 = \nabla^2 - \frac{\partial^2}{\partial z^2}$. The TE modes are derived from the corresponding eigenvalue problem with a homogeneous Neumann boundary condition,

$$\begin{cases} \nabla_T^2 v_{1n}(\boldsymbol{\rho}) + k_{t1n}^2 v_{1n}(\boldsymbol{\rho}) = 0, & \boldsymbol{\rho} \in \Omega, \\ \frac{\partial v_{1n}}{\partial n}(\boldsymbol{\rho}) = 0, & \boldsymbol{\rho} \in \Gamma. \end{cases} \quad (3.2)$$

The sets of eigenfunctions $\{v_{ln}\}_{n=1}^{\infty}$ are complete and orthogonal. We normalize them as

$$\iint_{\Omega} v_{ln}(\boldsymbol{\rho}) v_{ln'}(\boldsymbol{\rho}) dx dy = \delta_{n,n'}. \quad (3.3)$$

The electric fields corresponding to the eigenfunctions are given by

$$\mathbf{E}_{ln}^{\pm}(\mathbf{r}, \omega) = \begin{cases} \mathbf{E}_{ln}^T(\boldsymbol{\rho}, \omega) e^{\pm i k_{zln} z}, & l = 1 \text{ (TE mode)}, \\ (\mathbf{E}_{ln}^T(\boldsymbol{\rho}, \omega) \pm v_{ln}(\boldsymbol{\rho}) \hat{z}) e^{\pm i k_{zln} z}, & l = 2 \text{ (TM mode)}, \end{cases} \quad (3.4)$$

where the transverse eigenmodes are given by

$$\mathbf{E}_{ln}^T(\boldsymbol{\rho}, \omega) = \frac{i}{k_{tln}^2(\omega)} \begin{cases} -k(\omega) \eta(\omega) \hat{z} \times \nabla_T v_{ln}(\boldsymbol{\rho}), & l = 1 \text{ (TE mode)}, \\ k_{zln}(\omega) \nabla_T v_{ln}(\boldsymbol{\rho}), & l = 2 \text{ (TM mode)}. \end{cases} \quad (3.5)$$

The magnetic fields corresponding to the eigenfunctions are given by

$$\eta_0 \mathbf{H}_{ln}^{\pm}(\mathbf{r}, \omega) = \begin{cases} (\pm \eta_0 \mathbf{H}_{ln}^T(\boldsymbol{\rho}, \omega) + v_{ln}(\boldsymbol{\rho}) \hat{z}) e^{\pm i k_{zln} z}, & l = 1 \text{ (TE mode)}, \\ \pm \eta_0 \mathbf{H}_{ln}^T(\boldsymbol{\rho}, \omega) e^{\pm i k_{zln} z}, & l = 2 \text{ (TM mode)}, \end{cases} \quad (3.6)$$

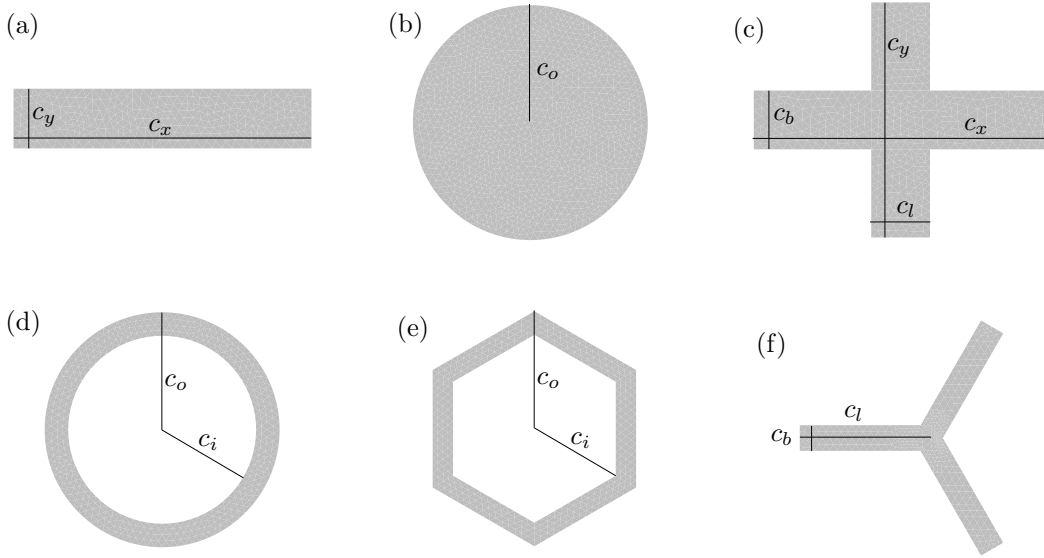


Figure 4: Examples of geometries for the waveguide: (a) Rectangular. (b) Circular. (c) Cross. (d) Annular. (e) Hexagonal. (f) Tripole.

where the transverse eigenmodes are given by

$$\eta_0 \mathbf{H}_{ln}^T(\boldsymbol{\rho}, \omega) = \frac{i}{k_{ln}^2(\omega)} \begin{cases} k_{zln}(\omega) \nabla_T v_{ln}(\boldsymbol{\rho}), & l = 1 \text{ (TE mode)}, \\ \frac{k(\omega)}{\eta(\omega)} \hat{z} \times \nabla_T v_{ln}(\boldsymbol{\rho}), & l = 2 \text{ (TM mode)}. \end{cases} \quad (3.7)$$

The TEM mode exists if the cross-section contour Γ consists of more than one non-connected part, see Fig. 3(b) or 4(d,e). The field components for the TEM mode are derived from the Laplace equation with a Dirichlet boundary condition, see for example [4]. For a cross-section that consists of two parts Γ_1 and Γ_2 , the equation and boundary condition read

$$\begin{cases} \nabla_T^2 \psi(\boldsymbol{\rho}) = 0, & \boldsymbol{\rho} \in \Omega, \\ \psi(\boldsymbol{\rho}) = \psi_i, & \boldsymbol{\rho} \in \Gamma_i, \quad i = 1, 2, \end{cases} \quad (3.8)$$

where ψ_i is a real constant. We normalize the potential ψ as

$$\iint_{\Omega} \nabla_T \psi(\boldsymbol{\rho}) \cdot \nabla_T \psi(\boldsymbol{\rho}) \, dx \, dy = 1. \quad (3.9)$$

The corresponding electric and magnetic fields are given by

$$\begin{aligned} \mathbf{E}_{ln}^{\pm}(\mathbf{r}, \omega) &= \mathbf{E}_{ln}^T(\boldsymbol{\rho}, \omega) e^{\pm i k_{zln} z} \\ \mathbf{H}_{ln}^{\pm}(\mathbf{r}, \omega) &= \pm \mathbf{H}_{ln}^T(\boldsymbol{\rho}, \omega) e^{\pm i k_{zln} z} \end{aligned} \quad l = 0 \text{ (TEM mode)}, \quad (3.10)$$

where the corresponding transverse electric and magnetic fields are given by

$$\begin{aligned} \mathbf{E}_{ln}^T(\boldsymbol{\rho}, \omega) &= -\nabla_T \psi(\boldsymbol{\rho}), \\ \pm \eta_0 \mathbf{H}_{ln}^T(\boldsymbol{\rho}, \omega) &= \mp \frac{1}{\eta(\omega)} \hat{z} \times \nabla_T \psi(\boldsymbol{\rho}), \end{aligned} \quad l = 0 \text{ (TEM mode)}. \quad (3.11)$$

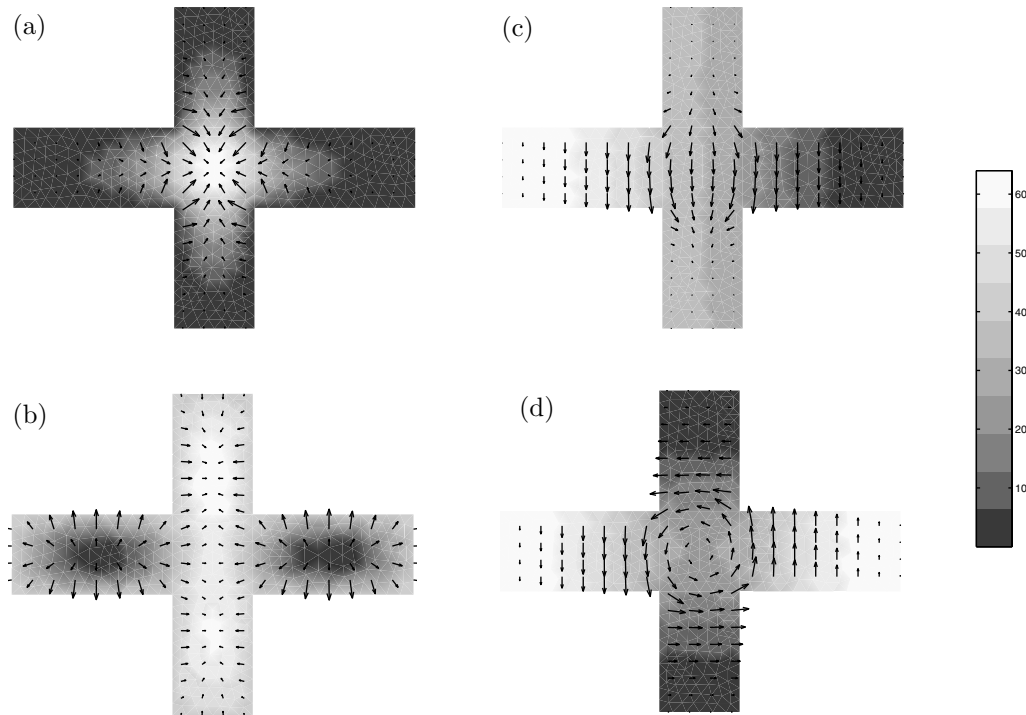


Figure 5: Examples of modes and fields in a cross-shaped waveguide: (a) The lowest TM mode. (b) The third TM mode. (c) The lowest TE mode. (d) The second TE mode.

The magnetic waveguide modes can be expressed in electric waveguide modes as

$$-\eta(\omega)\eta_0\hat{z} \times \mathbf{H}_{ln}^T(\boldsymbol{\rho}, \omega) = \begin{cases} \mathbf{E}_{ln}^T(\boldsymbol{\rho}, \omega), & l = 0 \text{ (TEM mode)}, \\ \frac{k_{zln}}{k(\omega)} \mathbf{E}_{ln}^T(\boldsymbol{\rho}, \omega), & l = 1 \text{ (TE mode)}, \\ \frac{k(\omega)}{k_{zln}} \mathbf{E}_{ln}^T(\boldsymbol{\rho}, \omega), & l = 2 \text{ (TM mode)}. \end{cases} \quad (3.12)$$

3.2 Known waveguide modes

In the previous section we saw that one can obtain the transverse electric fields $\mathbf{E}_{ln}^T(\boldsymbol{\rho}, \omega)$ for the waveguide modes by first solving the eigenvalue problems in Eqs. (3.2), (3.1) and then using Eq. (3.5). If the TEM mode is involved we also need to solve Eq. (3.8) and use Eq. (3.11). In Figure 4 we have depicted six examples of cross-sections for a waveguide. For simple geometries, *e.g.*, rectangular, circular and annular, there are well-known analytic expressions for the waveguide modes, cf. [2]. Structures with rectangular apertures are treated in Appendix A and structures with circular apertures with inner conductor are treated in Appendix B.

3.3 Unknown modes and FEM

For waveguides with more complicated cross-sections there are generally no closed form expressions for the waveguide fields. Instead these fields need to be determined numerically, and in this paper we utilize the FEM for this purpose. FEM is a very suitable method for the two-dimensional eigenvalue problems in Eqs. (3.2) and (3.1). A simple and quick introduction to the application of FEM to electromagnetic problems is given in [6].

There are several commercial FEM programs that are suited for two-dimensional eigenvalue problems. We have chosen FEMLAB, see [3], which is a toolbox to MATLAB. FEMLAB provides graphic tools to describe complicated domains and it automatically generates triangular meshes. It also discretizes the PDEs, finds discrete solutions and plots the results.

Figure 5 shows four examples of waveguide modes for a cross-shaped waveguide. In (a) and (b) we plot the lowest and the third TM mode, and in (c) and (d) we plot the lowest and the second TE mode. The gray scale in Figure 5 illustrates the solution to the eigenvalue problem, $v_{2n}(\boldsymbol{\rho})$ in (3.1) for the TM modes and $v_{1n}(\boldsymbol{\rho})$ in (3.2) for the TE modes. The arrows in the Figure 5 show the corresponding transverse electric field \mathbf{E}_{1n}^T , see (3.5).

4 Numerical results

4.1 Measured and calculated transmission

In this section we compare measured and calculated transmission for a copper sheet, that is perforated with rectangular apertures, see Figure 4. The sheet is 1.1 mm thick and the rectangular apertures are $c_x = 18.0$ mm wide and $c_y = 5.5$ mm high. The rectangular apertures are oriented such that the x -axis is parallel to the long side. The periodicity is given by $a = 23.25$ mm, $b = 15.55$ mm and $\phi_0 = 90^\circ$.

In Figure 6 we present the measured and calculated transmitted power for TM-incidence with the azimuthal angle $\phi = 90^\circ$. The computed curves are calculated with both known waveguide modes (see Appendix A) and modes produced by FEM. In the calculations we use Floquet waves with index $|m|, |n| \leq 10$, *i.e.*, the number of Floquet waves are $2(2 \times 10 + 1)^2 = 882$. When we use known waveguide modes we take modes with highest index 5, *i.e.*, 60 modes, and when we use FEM modes we take the 14 lowest propagating modes, *i.e.*, TE₁₀, TE₂₀, TE₃₀, TE₀₁, TE₁₁, TE₂₁, TE₄₀, TE₃₁, TE₅₀, TE₄₁, TM₁₁, TM₂₁, TM₃₁, TM₄₁. The cutoff frequency for the first propagating mode, *i.e.*, TE₁₀, is $f_{cutoff} = 8.33$ GHz. No other modes propagate in the current frequency band, 8 – 12 GHz.

We see from Figure 6 that we have good agreement between measured and computed power transmission and between curves which are calculated with known waveguide modes and modes produced by the FEM.

Figure 6 also shows how the transmission depends on the angle of incident. Since we plot the power transmission for three different angles $\theta = 0^\circ, 30^\circ, 60^\circ$, we can see that the passband for the transmission is falling in frequency then the angle of

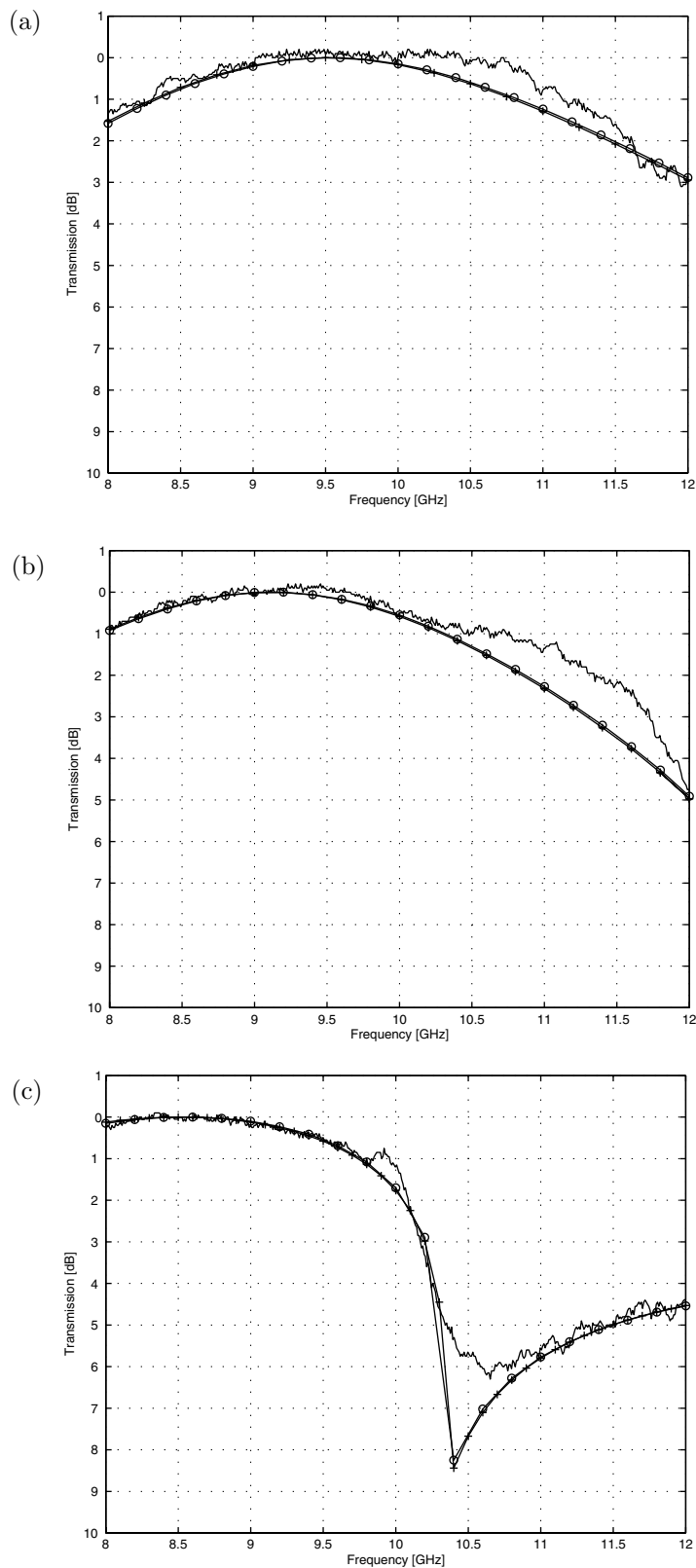


Figure 6: Comparison between measured and calculated transmission. The curves show the power transmission coefficient for TM-incidence on a screen perforated with rectangular apertures as a function of frequency. The solid curve is measured, the curve with rings is calculated with known waveguide modes and the curve with the cross is calculated with FEM modes. (a) $\theta = 0^\circ$, (b) $\theta = 30^\circ$, (c) $\theta = 60^\circ$.

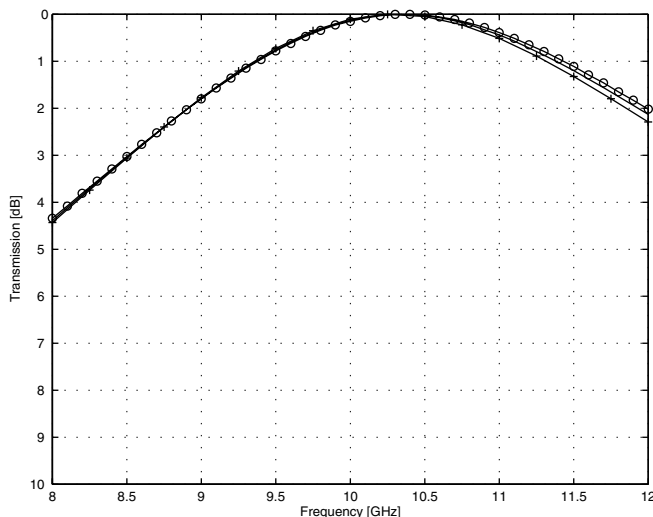


Figure 7: Comparison between different methods for calculating the transmission. The curves show the power transmission coefficient for TE-incidence on a screen perforated with annular apertures as a function of frequency. The solid curve is calculated with the spectral Galerkin method, the curve with rings is calculated with known waveguide modes and the curve with the cross is calculated with FEM modes.

incident increases.

4.2 Thin screens (FSS)

In this subsection we investigate how the present method handles thin screens, *i.e.*, frequency selective surfaces. Numerous methods have been used to analyze thin screens, among other, we mention the equivalent circuit method, the mutual-impedance method and the integral equation method [13]. Here, we compare the present method with an integral equation method called the spectral Galerkin method [12]. In the spectral Galerkin method the thickness of the screen is assumed to be zero. We consider a screen with thickness $18 \mu\text{m}$, perforated with annular apertures. The chosen thickness, $18 \mu\text{m}$, is a typical thickness of the copper layer on the printed circuit board, often used in FSS measurements.

In Figure 7 the power transmission for a thin screen with annular apertures is depicted, see Figure 4. The outer radius is $c_o = 6 \text{ mm}$ and the inner radius is $c_i = 5 \text{ mm}$. The periodicity is given by $a = 24.40 \text{ mm}$, $b = 17.25 \text{ mm}$ and $\phi_0 = 45^\circ$. The structure is illuminated with a TE-polarized plane wave at normal incidence, *i.e.*, $\theta = \phi = 0$. Three curves are presented in Figure 7 and these are calculated with three different methods. One curve is calculated with the spectral Galerkin method [12], where the thickness of the structure is assumed to be zero, that is $h = 0$. The other two curves are obtained by mode matching with known waveguide modes (see Appendix B) and modes produced by FEM. In both calculations we use

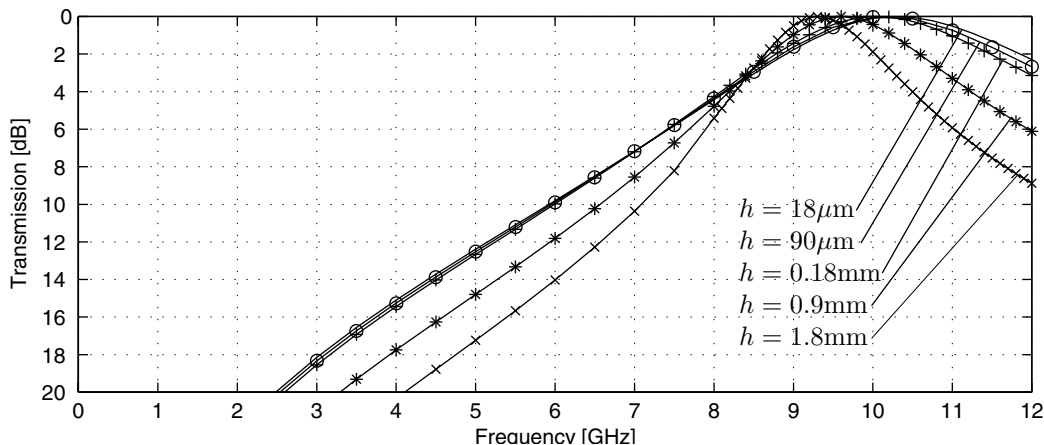


Figure 8: The dependence of thickness. The curves show the power transmission coefficient as a function of frequency, for a TE-wave incident on a screen perforated with annular apertures. The thicknesses of the screens are indicated in the figure.

the thickness $h = 18 \mu\text{m}$. We use Floquet waves with index $|m|, |n| \leq 14$, *i.e.*, the number of Floquet waves are $2(2 \times 14 + 1)^2 = 1682$. When we use known modes we take modes with highest index 5, corresponding to 120 modes, and when we use FEM modes we take the 19 lowest propagating modes.

Since the aperture have a annular cross-section that consist of two non-connecting parts, a TEM mode can propagate in the aperture. The TEM mode propagates for all frequencies, and the cutoff frequency for the next propagating mode (a double mode) is $f_{cutoff} = 8.7 \text{GHz}$. No other modes propagate in the current frequency band, $0 - 12 \text{GHz}$.

Figure 7 verifies the present method for thin screens. Notice that more waveguide modes are needed to obtain correct result when the structure is thin, compared to thicker screens. This depends on the fact that the evanescent modes (modes that decrease exponentially) contribute more for thin structures. The number of modes is determined by adding modes until the result does not change.

4.3 Thick screens

In this subsection we investigate how the transmission depends on the thickness of the screen. In Figure 8 we see the power transmission for a structure with annular apertures. We have used the same parameters as in Section 4.2, except that we let the thickness vary from $h = 18 \mu\text{m}$ to 1.8mm . We see that the bandwidth decreases when the thickness of the screen is increased, and that the passband is falling slightly in frequency when the screen becomes thicker. It is also concluded that if h is smaller than 0.18mm , we have moderate changes in the transmission.

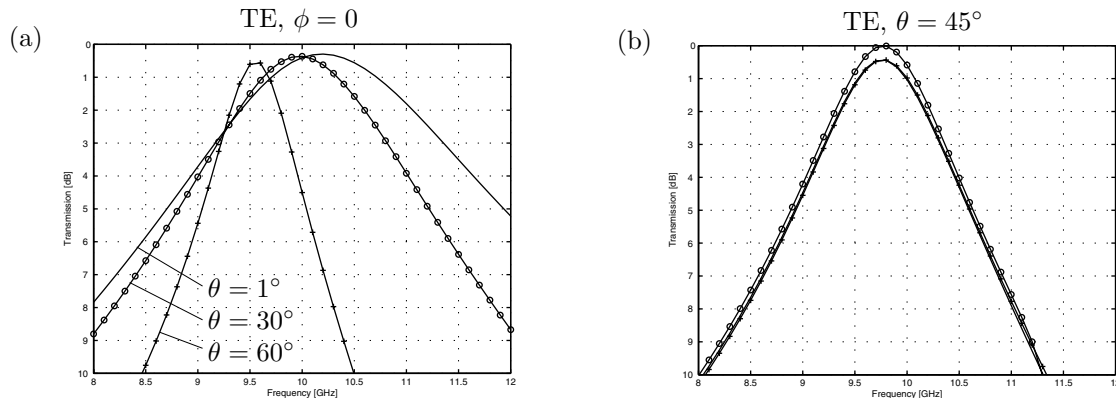


Figure 9: Transmission through hexagonal apertures. The curves shows the power transmission coefficient for TE-incidence as a function of frequency. In (a) we have $\phi = 0^\circ$ and varying θ ; 1° , 30° , 60° , and in (b) we have $\theta = 45^\circ$ and varying ϕ ; 0° , 30° , 60° .

4.4 Hexagonal and tripole apertures

In this section we investigate the transmission of two types of screens with complex geometries, namely hexagonal and tripole apertures, see Figure 4. In these cases we do not have any closed form expressions for the waveguide fields. Therefore we calculate the waveguide fields numerically by the FEM.

In Figure 9, the power transmission of a thick screen perforated with hexagonal apertures is depicted, see Figure 4. The outer radius is $c_o = 6$ mm, the inner radius is $c_i = 5$ mm and the thickness is $h = 1.1$ mm. The periodicity is given by $a = 18$ mm, $b = 18$ mm and $\phi_0 = 60^\circ$. Figure 9(b) indicates that the band of transmission is independent of ϕ .

Since the aperture have a hexagonal cross-section that consist of two non-connecting parts, a TEM mode can propagate in the aperture. The TEM mode propagates for all frequencies, and the cutoff frequency for the next propagating mode (a double mode) is $f_{cutoff} = 10.0$ GHz. No other modes propagate in the current frequency band, 8 – 12 GHz. In the calculations we have used Floquet waves with index $|m|, |n| \leq 4$, and the 6 lowest propagating modes.

In Figure 10 we see the power transmission of a thick screen perforated with the tripole apertures depicted in Figure 4(f). The length is $c_l = 7.5$ mm, the width is $c_b = 0.5$ mm and the thickness is $h = 1.1$ mm. The periodicity is given by $a = 15$ mm, $b = 15$ mm and $\phi_0 = 60^\circ$. The structure is illuminated with both a TE- and a TM-polarized plane wave. In Figure 10(a) and (b) we have $\phi = 0^\circ$ and a varying $\theta = 1^\circ, 20^\circ, 40^\circ, 60^\circ$. The Figure 10(a) shows that the bandwidth becomes narrower for TE when we increase the angle of incidence, but in Figure 10(b) we can see that the bandwidth becomes broader for TM when we increase the angle of incidence. In Figures 10(c) and (d) we have $\theta = 45^\circ$ and a varying $\phi = 0^\circ, 15^\circ, 30^\circ, 60^\circ$. The Figures 10(c) and (d) show that the band of transmission is independent of ϕ .

In the tripole aperture can no TEM mode propagate, since the cross-section

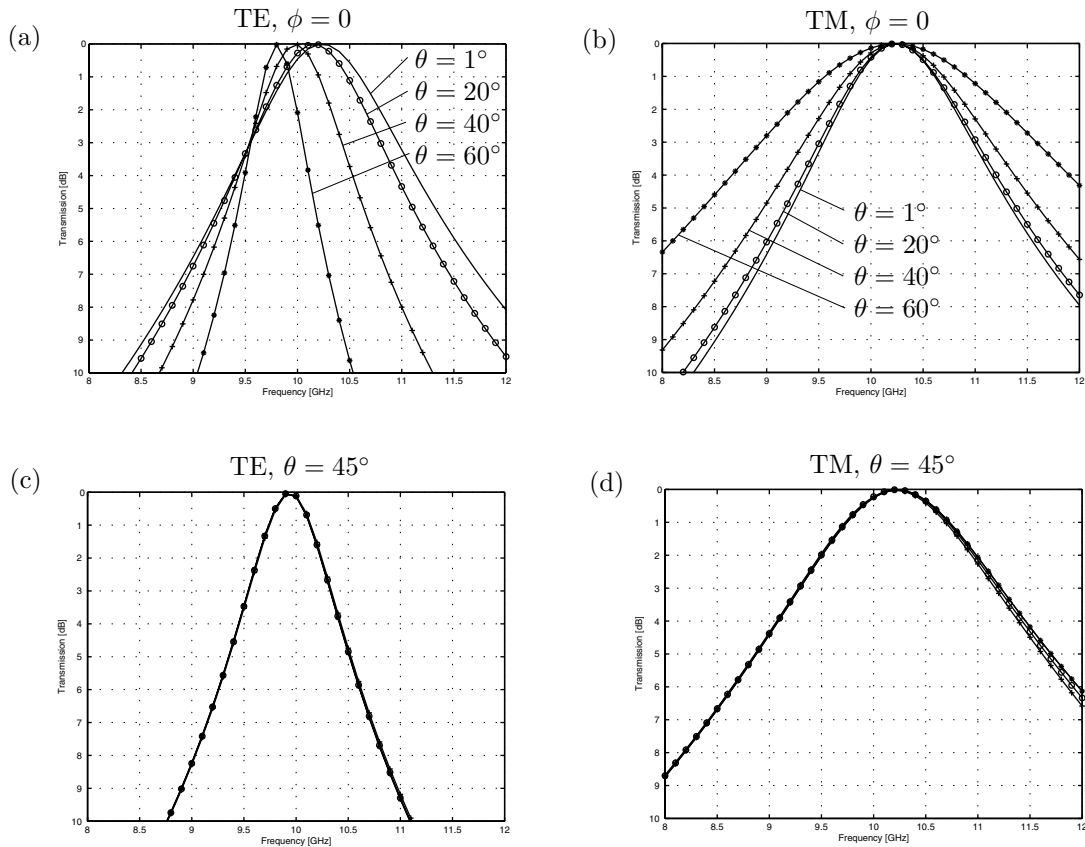


Figure 10: Transmission through tripole apertures. The curves show the power transmission coefficient as a function of frequency. In (a) and (c) we have TE-incidence, and in (b) and (d) we have TM-incidence. In (a) and (b) we have $\phi = 0^\circ$ and varying θ ; $1^\circ, 20^\circ, 40^\circ, 60^\circ$. In (c) and (d) we have $\theta = 45^\circ$ and varying ϕ ; $0^\circ, 15^\circ, 30^\circ, 60^\circ$.

consist of only one simply connecting parts. The cutoff frequency for the first propagating mode (a double mode) is $f_{cutoff} = 9.22$ GHz. No other modes propagate in the current frequency band, 8 – 12 GHz. In the calculations we have used Floquet waves with index $|m|, |n| \leq 2$, and the 5 lowest propagating modes.

If we compare Figure 9 and 10 we see that hexagonal apertures have larger bandwidth than tripole apertures.

5 Conclusions

In this paper thick screens perforated with periodic arrays of apertures are considered. The fields outside the structure are expanded in plane waves, while the field inside the apertures are expanded in appropriate waveguide modes. The boundary conditions for the tangential electric and magnetic fields are applied to get a linear system of equations for the coefficients of the waveguide modes. We solve this system of equations by matrix inversion, and obtain the transmitted and reflected fields.

Four geometries of the apertures are considered in the numerical calculations, namely rectangular, annular, tripole, and hexagonal. For respective case we have calculated the transmission as a function of frequency. For a thick structure (1.1 mm) perforated with rectangular apertures, excellent agreement with measurements was found. We also calculated the transmission for extreme thin structures (18 μm). The result of the present method was in accordance with the result of an established integral equation method, *i.e.*, the spectral Galerkin method [12], where the thickness of the screen is assumed to be zero. Hence, the present method was verified for thin structures. We have also investigate how the transmission depends on the thickness of the screen. It is concluded that the bandwidth decreases when the thickness of the screen is increased. Finally, we studied the transmission of two types of screen with complex geometries, namely hexagonal and tripole apertures. In all computations we have stated how many Floquet waves and waveguide modes we need for the result to converge.

In context of thickness dependence, it has been discussed if one can use a carbon fabric instead of copper layer in conventional (thin) FSS structures. A carbon fabric is thicker than a copper layer ($\approx 18 \mu\text{m}$). We have used the method in this paper to see if thickness has any important effect. The conductivity of the carbon fabric is finite, but was in the calculations approximated with an infinite conductivity.

The conclusions from the study is that thick screens are appropriate for low observable radomes with small bandwidth. The transmission inside the band is very good, attenuation outside the band is extremely good and the angle of incidence dependence is acceptable. However, for radomes where moderate or large bandwidth is required, a patch which partly covers the aperture area should be included at each end of the aperture, forming a so called artificial puck plate (APP) structure [13]. These APP structures have excellent properties regarding bandwidth, scan independence and polarisation independence [13]. This project is to be considered as a first step of the development of a computer code for APP structures with

arbitrary cross-section.

6 Acknowledgments

We would like to thank the Defense Materiel Administration in Sweden for financial support. Furthermore, we would like to thank Applied Composites AB, ACAB, for the measurements.

Appendix A Rectangular apertures

When the apertures are rectangular, the field in the apertures can be expanded in classical waveguide modes, which usually are used to describe the field in a rectangular waveguide. The rectangular apertures are right-angled and the sides of apertures are parallel with the x - and the y -axis, respectively. The width of the apertures (along the x -axis) is denoted c_x , while the height is denoted c_y . The waveguide modes \mathbf{E}_{lmn}^T are defined as, see for example [2],

$$\begin{aligned}\mathbf{E}_{1mn}^T(\boldsymbol{\rho}) &:= g_{mn} \left[\hat{x} \frac{n\pi}{c_y} \cos\left(\frac{m\pi x}{c_x}\right) \sin\left(\frac{n\pi y}{c_y}\right) - \hat{y} \frac{m\pi}{c_x} \sin\left(\frac{m\pi x}{c_x}\right) \cos\left(\frac{n\pi y}{c_y}\right) \right], \\ \mathbf{E}_{2mn}^T(\boldsymbol{\rho}) &:= g_{mn} \left[\hat{x} \frac{m\pi}{c_x} \cos\left(\frac{m\pi x}{c_x}\right) \sin\left(\frac{n\pi y}{c_y}\right) + \hat{y} \frac{n\pi}{c_y} \sin\left(\frac{m\pi x}{c_x}\right) \cos\left(\frac{n\pi y}{c_y}\right) \right],\end{aligned}$$

where $g_{mn} := ((2 - \delta_{m0})(2 - \delta_{n0})/c_x c_y)^{1/2} ((m\pi/c_x)^2 + (n\pi/c_y)^2)^{-1/2}$ is a factor of normalization. The waveguide modes are orthonormal in the meaning that

$$\int_{\Omega} \mathbf{E}_{lmn}^T(\boldsymbol{\rho}) \cdot \mathbf{E}_{l'm'n'}^T(\boldsymbol{\rho}) \, dx \, dy = \delta_{ll'} \delta_{mm'} \delta_{nn'}.$$

Note that $l = 1$ corresponds to the TE modes, while $l = 2$ corresponds to the TM modes. For TE modes $m = 0, 1, 2, \dots$, $n = 0, 1, 2, \dots$ and $(m, n) \neq (0, 0)$, and for TM modes $m = 1, 2, \dots$ and $n = 1, 2, \dots$. For rectangular apertures $k_{zp} := (k^2 - (m\pi/c_x)^2 - (n\pi/c_y)^2)^{1/2}$, see (2.5).

A.1 Convolutions

In this section we consider the convolution between the rectangular waveguide modes and the Floquet waves, *i.e.*, $\mathbf{E}_{lmn}^T * \mathbf{R}_{l'm'n'}$, which we have defined as

$$\mathbf{E}_{lmn}^T * \mathbf{R}_{l'm'n'} = \int_S \mathbf{E}_{lmn}^T(\boldsymbol{\rho}) \cdot \mathbf{R}_{l'm'n'}(\boldsymbol{\rho}) \, dx \, dy,$$

where Ω is the cross-section of the waveguide, $\Omega = \{0 < x < c_x, 0 < y < c_y\}$. Since the space dependence in both the waveguide modes and the Floquet waves can be

expressed in exponential functions, the integral above can be calculated analytically. The following integrals are useful

$$\begin{aligned}\Gamma_m^{(1)}(\alpha, c) &:= \int_0^c \cos(m\pi\xi/c)e^{-i\alpha\xi} d\xi, \\ \Gamma_m^{(2)}(\alpha, c) &:= \int_0^c \sin(m\pi\xi/c)e^{-i\alpha\xi} d\xi.\end{aligned}$$

We replace the cosine- and the sinus functions with (complex) exponential functions and get

$$\begin{aligned}\Gamma_m^{(1)}(\alpha, c) &= \frac{ic^2\alpha(1 - (-1)^m e^{-i\alpha c})}{m^2\pi^2 - \alpha^2 c^2}, \\ \Gamma_m^{(2)}(\alpha, c) &= \frac{cm\pi(1 - (-1)^m e^{-i\alpha c})}{m^2\pi^2 - \alpha^2 c^2}.\end{aligned}$$

Thus the explicit expressions for the convolutions read

$$\begin{aligned}\mathbf{E}_{1mn}^T * \mathbf{R}_{1m'n'} &= \frac{g_{mn}}{\sqrt{A_S}} \left(\frac{n\pi}{c_y} \frac{\beta_{m'n'}}{\tau_{m'n'}} \Gamma_1 + \frac{m\pi}{c_x} \frac{\alpha_{m'}}{\tau_{m'n'}} \Gamma_2 \right), \\ \mathbf{E}_{1mn}^T * \mathbf{R}_{2m'n'} &= \frac{g_{mn}}{\sqrt{A_S}} \left(\frac{n\pi}{c_y} \frac{\alpha_{m'}}{\tau_{m'n'}} \Gamma_1 - \frac{m\pi}{c_x} \frac{\beta_{m'n'}}{\tau_{m'n'}} \Gamma_2 \right), \\ \mathbf{E}_{2mn}^T * \mathbf{R}_{1m'n'} &= \frac{g_{mn}}{\sqrt{A_S}} \left(\frac{m\pi}{c_x} \frac{\beta_{m'n'}}{\tau_{m'n'}} \Gamma_1 - \frac{n\pi}{c_y} \frac{\alpha_{m'}}{\tau_{m'n'}} \Gamma_2 \right), \\ \mathbf{E}_{2mn}^T * \mathbf{R}_{2m'n'} &= \frac{g_{mn}}{\sqrt{A_S}} \left(\frac{m\pi}{c_x} \frac{\alpha_{m'}}{\tau_{m'n'}} \Gamma_1 + \frac{n\pi}{c_y} \frac{\beta_{m'n'}}{\tau_{m'n'}} \Gamma_2 \right),\end{aligned}$$

where $\Gamma_1 := \Gamma_m^{(1)}(\alpha_{m'}, c_x)\Gamma_n^{(2)}(\beta_{m'n'}, c_y)$ and $\Gamma_2 := \Gamma_m^{(2)}(\alpha_{m'}, c_x)\Gamma_n^{(1)}(\beta_{m'n'}, c_y)$.

Appendix B Annular apertures

Another well-known waveguide geometry is the coaxial cable. The cable has concentric circular inner and outer conductors. The fields propagate between the conductors. The coaxial cable can, unlike the rectangular waveguide, support a mode, the TEM mode, which propagates for all frequencies. The radii of the outer and inner boundary surface are denoted ρ_a and ρ_b , respectively. We introduce the dimensionless quantity $d := \rho_a/\rho_b$, which always is greater than one, $d > 1$. Before we define the waveguide modes, we do some definitions. We let χ_{mn} be the zeros to the function $J_m(dx)Y_m(x) - Y_m(dx)J_m(x)$, where $J_m(x)$ and $Y_m(x)$ are Bessel functions of the first and second kind, respectively. We have that $m \geq 0$, while $n \geq 1$. Further we let χ'_{mn} be the zeros to the function $J'_m(dx)Y'_m(x) - Y'_m(dx)J'_m(x)$. The zeros χ_{mn} and χ'_{mn} are determined numerically, by *e.g.*, the Newton-Raphsons method. Numerical values of χ_{mn} and χ'_{mn} , for different values of d , are given by Marcuvitz [5]. We also define the functions

$$Z_m\left(\frac{\chi_{mn}\rho}{\rho_b}\right) := \frac{\sqrt{\pi\varepsilon_m}}{2} \frac{J_m\left(\frac{\chi_{mn}\rho}{\rho_b}\right)Y_m(\chi_{mn}) - Y_m\left(\frac{\chi_{mn}\rho}{\rho_b}\right)J_m(\chi_{mn})}{\sqrt{\left(\frac{J_m(\chi_{mn})}{J_m(d\chi_{mn})}\right)^2 - 1}}$$

and

$$I_m\left(\frac{\chi'_{mn}\rho}{\rho_b}\right) := \frac{\sqrt{\pi\varepsilon_m}}{2} \frac{J_m\left(\frac{\chi'_{mn}\rho}{\rho_b}\right)Y'_m(\chi'_{mn}) - Y_m\left(\frac{\chi'_{mn}\rho}{\rho_b}\right)J'_m(\chi'_{mn})}{\sqrt{\left(\frac{J'_m(\chi'_{mn})}{J'_m(d\chi'_{mn})}\right)^2 \left(1 - \left[\frac{m}{d\chi'_{mn}}\right]^2\right) - \left(1 - \left[\frac{m}{\chi'_{mn}}\right]^2\right)}},$$

where $\varepsilon_m := 2 - \delta_{m0}$.

The TEM mode we define as

$$\mathbf{E}_{000}^T(\boldsymbol{\rho}) := \frac{1}{\sqrt{2\pi \log d}} \hat{\boldsymbol{\rho}},$$

while the remaining modes are given by

$$\begin{aligned} \mathbf{E}_{1mn1}^T(\boldsymbol{\rho}) &:= \frac{m}{\rho} I_m\left(\frac{\chi'_{mn}\rho}{\rho_b}\right) \sin(m\phi) \hat{\boldsymbol{\rho}} + \frac{\chi'_{mn}}{\rho_b} I'_m\left(\frac{\chi'_{mn}\rho}{\rho_b}\right) \cos(m\phi) \hat{\boldsymbol{\phi}}, \\ \mathbf{E}_{1mn2}^T(\boldsymbol{\rho}) &:= -\frac{m}{\rho} I_m\left(\frac{\chi'_{mn}\rho}{\rho_b}\right) \cos(m\phi) \hat{\boldsymbol{\rho}} + \frac{\chi'_{mn}}{\rho_b} I'_m\left(\frac{\chi'_{mn}\rho}{\rho_b}\right) \sin(m\phi) \hat{\boldsymbol{\phi}}, \\ \mathbf{E}_{2mn1}^T(\boldsymbol{\rho}) &:= -\frac{\chi_{mn}}{\rho_b} Z'_m\left(\frac{\chi_{mn}\rho}{\rho_b}\right) \sin(m\phi) \hat{\boldsymbol{\rho}} - \frac{m}{\rho} Z_m\left(\frac{\chi_{mn}\rho}{\rho_b}\right) \cos(m\phi) \hat{\boldsymbol{\phi}} \end{aligned}$$

and

$$\mathbf{E}_{2mn2}^T(\boldsymbol{\rho}) := -\frac{\chi_{mn}}{\rho_b} Z'_m\left(\frac{\chi_{mn}\rho}{\rho_b}\right) \cos(m\phi) \hat{\boldsymbol{\rho}} + \frac{m}{\rho} Z_m\left(\frac{\chi_{mn}\rho}{\rho_b}\right) \sin(m\phi) \hat{\boldsymbol{\phi}},$$

where $m \geq 0$ and $n \geq 1$. The modes \mathbf{E}_{lmns}^T form a complete system over the aperture $\rho_b \leq \rho \leq \rho_a$ and $0 \leq \phi < 2\pi$. As before $l = 1$ and $l = 2$ represent TE and TM modes, respectively. The index s indicates if the mode is horizontal ($s = 1$) or vertical ($s = 2$). A horizontal mode has no ϕ -component on the x -axis, while a vertical mode has no ρ -component on the x -axis. Finally the modes are orthonormal in the meaning that

$$\int_{\rho_b}^{\rho_a} \int_0^{2\pi} \mathbf{E}_{lmns}^T(\boldsymbol{\rho}) \cdot \mathbf{E}_{l'm'n's'}^T(\boldsymbol{\rho}) \rho \, d\rho \, d\phi = \delta_{ll'} \delta_{mm'} \delta_{nn'} \delta_{ss'}.$$

B.1 Convolutions

The convolution between a waveguide mode $\mathbf{E}_{lmns}^T(\boldsymbol{\rho})$, for a coaxial cable, and a Floquet wave $\mathbf{R}_{l'm'n'}(\boldsymbol{\rho})$ is defined as

$$\mathbf{E}_{lmns}^T * \mathbf{R}_{l'm'n'} := \int_{\rho_b}^{\rho_a} \rho \, d\rho \int_0^{2\pi} d\phi \mathbf{E}_{lmns}^T(\boldsymbol{\rho}) \cdot \mathbf{R}_{l'm'n'}^*(\boldsymbol{\rho}).$$

We note that the Floquet waves can be written as

$$\begin{aligned} \mathbf{R}_{1mn}^*(\boldsymbol{\rho}) &= \frac{\hat{x} \sin \varphi_{mn} - \hat{y} \cos \varphi_{mn}}{\sqrt{A_S}} e^{-i\rho\tau_{mn} \cos(\phi - \varphi_{mn})}, \\ \mathbf{R}_{2mn}^*(\boldsymbol{\rho}) &= \frac{\hat{x} \cos \varphi_{mn} + \hat{y} \sin \varphi_{mn}}{\sqrt{A_S}} e^{-i\rho\tau_{mn} \cos(\phi - \varphi_{mn})} \end{aligned}$$

or

$$\begin{aligned}\mathbf{R}_{1mn}^*(\boldsymbol{\rho}) &= -\frac{\hat{\rho} \sin(\phi - \varphi_{mn}) + \hat{\phi} \cos(\phi - \varphi_{mn})}{\sqrt{A_S}} e^{-i\rho\tau_{mn} \cos(\phi - \varphi_{mn})}, \\ \mathbf{R}_{2mn}^*(\boldsymbol{\rho}) &= \frac{\hat{\rho} \cos(\phi - \varphi_{mn}) - \hat{\phi} \sin(\phi - \varphi_{mn})}{\sqrt{A_S}} e^{-i\rho\tau_{mn} \cos(\phi - \varphi_{mn})},\end{aligned}$$

where we have introduced τ_{mn} and φ_{mn} as the polar coordinates for the vector $\boldsymbol{\tau}_{mn}$,

$$\begin{cases} \alpha_m = \tau_{mn} \cos \varphi_{mn}, \\ \beta_{mn} = \tau_{mn} \sin \varphi_{mn}. \end{cases}$$

In the following section we derive all the convolutions which we need for the numerical calculations, see also thesis [8]. As an alternative to these relatively long derivations one can present a short handbook over the convolutions. The disadvantage with such a handbook is that it is of no value if it contains misprints and therefore we have chosen to give the derivations.

B.1.1 TEM mode

First we consider the convolution between the TEM mode and a Floquet wave. We note that

$$\rho \mathbf{E}_{0000}^T(\boldsymbol{\rho}) = \frac{\hat{\rho}}{\sqrt{2\pi \log c}},$$

and hence

$$\begin{aligned}\mathbf{E}_{0000}^T * \mathbf{R}_{1m'n'} &= -\int_{\rho_b}^{\rho_a} d\rho \int_0^{2\pi} d\phi \frac{\sin(\phi - \varphi_{mn})}{\sqrt{2\pi A_S \log c}} e^{-i\rho\tau_{mn} \cos(\varphi_{mn} - \phi)}, \\ \mathbf{E}_{0000}^T * \mathbf{R}_{2m'n'} &= \int_{\rho_b}^{\rho_a} d\rho \int_0^{2\pi} d\phi \frac{\cos(\phi - \varphi_{mn})}{\sqrt{2\pi A_S \log c}} e^{-i\rho\tau_{mn} \cos(\varphi_{mn} - \phi)}.\end{aligned}$$

The integration over ρ can be done easily and we get

$$\begin{aligned}\mathbf{E}_{0000}^T * \mathbf{R}_{1m'n'} &= \frac{-i}{\sqrt{2\pi A_S \log c}} \int_0^{2\pi} \tan \phi (e^{-i\rho_b \tau_{mn} \cos \phi} - e^{-i\rho_a \tau_{mn} \cos \phi}) d\phi, \\ \mathbf{E}_{0000}^T * \mathbf{R}_{2m'n'} &= \frac{i}{\sqrt{2\pi A_S \log c}} \int_0^{2\pi} (e^{-i\rho_b \tau_{mn} \cos \phi} - e^{-i\rho_a \tau_{mn} \cos \phi}) d\phi,\end{aligned}$$

where we have replaced $\phi - \varphi$ with ϕ . This replacement can be done thanks to integration over a whole period. The first integral is zero, since the integrand is odd. The second integral can be calculated with help of

$$\int_0^{2\pi} e^{-i\xi \cos \phi} d\phi = \int_0^{2\pi} \cos(\xi \cos \phi) d\phi = 2\pi J_0(\xi),$$

where in the last identity we have used 9.1.18 in *Handbook of Mathematical Functions* [1]. To sum up we have

$$\begin{aligned}\mathbf{E}_{0000}^T * \mathbf{R}_{1m'n'} &= 0, \\ \mathbf{E}_{0000}^T * \mathbf{R}_{2m'n'} &= i\sqrt{\frac{2\pi}{A_S \log c}} \frac{J_0(\tau_{m'n'} \rho_a) - J_0(\tau_{m'n'} \rho_b)}{\tau_{m'n'}}.\end{aligned}$$

B.1.2 TE modes

We now consider the convolution between Floquet waves and TE modes, $\mathbf{E}_{1mns}^T(\boldsymbol{\rho})$. We have that

$$\begin{aligned} \mathbf{E}_{1mn1}^T * \mathbf{R}_{1m'n'} &= -\frac{1}{\sqrt{A_S}} \int_{\rho_b}^{\rho_a} d\rho \int_0^{2\pi} d\phi \left\{ m I_m\left(\frac{\chi'_{mn}\rho}{\rho_b}\right) \sin(m\phi) \sin(\phi - \varphi_{m'n'}) \right. \\ &\quad \left. + \frac{\chi'_{mn}\rho}{\rho_b} I'_m\left(\frac{\chi'_{mn}\rho}{\rho_b}\right) \cos(m\phi) \cos(\phi - \varphi_{m'n'}) \right\} e^{-i\rho\tau_{m'n'} \cos(\phi - \varphi_{m'n'})}. \end{aligned}$$

We start with the variable substitution $\phi - \varphi_{m'n'} \rightarrow \phi$ and we get

$$\begin{aligned} \mathbf{E}_{1mn1}^T * \mathbf{R}_{1m'n'} &= -\frac{1}{\sqrt{A_S}} \int_{\rho_b}^{\rho_a} d\rho \int_{-\varphi_{m'n'}}^{2\pi - \varphi_{m'n'}} d\phi \\ &\quad \times \left\{ m I_m\left(\frac{\chi'_{mn}\rho}{\rho_b}\right) \sin(m(\phi + \varphi_{m'n'})) \sin \phi \right. \\ &\quad \left. + \frac{\chi'_{mn}\rho}{\rho_b} I'_m\left(\frac{\chi'_{mn}\rho}{\rho_b}\right) \cos(m(\phi + \varphi_{m'n'})) \cos \phi \right\} e^{-i\rho\tau_{m'n'} \cos \phi}. \end{aligned}$$

We use the relations

$$\begin{cases} \cos(m(\phi + \varphi_{m'n'})) = \cos(m\phi) \cos(m\varphi_{m'n'}) - \sin(m\phi) \sin(m\varphi_{m'n'}) \\ \sin(m(\phi + \varphi_{m'n'})) = \sin(m\phi) \cos(m\varphi_{m'n'}) + \cos(m\phi) \sin(m\varphi_{m'n'}) \end{cases} \quad (\text{B.1})$$

and note that ϕ -integral of odd integrands are zero. We have

$$\begin{aligned} \mathbf{E}_{1mn1}^T * \mathbf{R}_{1m'n'} &= -\frac{1}{\sqrt{A_S}} \cos(m\varphi_{m'n'}) \int_{\rho_b}^{\rho_a} d\rho \int_0^{2\pi} d\phi \\ &\quad \times \left\{ m I_m\left(\frac{\chi'_{mn}\rho}{\rho_b}\right) \sin(m\phi) \sin \phi \right. \\ &\quad \left. + \frac{\chi'_{mn}\rho}{\rho_b} I'_m\left(\frac{\chi'_{mn}\rho}{\rho_b}\right) \cos(m\phi) \cos \phi \right\} e^{-i\rho\tau_{m'n'} \cos \phi}, \end{aligned}$$

where we have changed the interval of integration to $0 \leq \phi \leq 2\pi$. Now we apply the relations

$$\begin{cases} \cos(m\phi) \cos \phi = \frac{1}{2} (\cos((m-1)\phi) + \cos((m+1)\phi)), \\ \sin(m\phi) \sin \phi = \frac{1}{2} (\cos((m-1)\phi) - \cos((m+1)\phi)), \end{cases} \quad (\text{B.2})$$

and use that the integrand is an even function of ϕ around $\phi = \pi$. We get

$$\begin{aligned} \mathbf{E}_{1mn1}^T * \mathbf{R}_{1m'n'} &= -\frac{1}{\sqrt{A_S}} \cos(m\varphi_{m'n'}) \int_{\rho_b}^{\rho_a} d\rho \int_0^{\pi} d\phi \\ &\quad \times \left\{ m I_m\left(\frac{\chi'_{mn}\rho}{\rho_b}\right) (\cos((m-1)\phi) - \cos((m+1)\phi)) \right. \\ &\quad \left. + \frac{\chi'_{mn}\rho}{\rho_b} I'_m\left(\frac{\chi'_{mn}\rho}{\rho_b}\right) (\cos((m-1)\phi) + \cos((m+1)\phi)) \right\} e^{-i\rho\tau_{m'n'} \cos \phi}. \end{aligned}$$

With the help of 9.1.21 in [1] we can do the integration over ϕ . We get

$$\begin{aligned} \mathbf{E}_{1mn1}^T * \mathbf{R}_{1m'n'} &= -\frac{\pi}{\sqrt{A_S}} \cos(m\varphi_{m'n'}) (-i)^{m-1} \\ &\times \int_{\rho_b}^{\rho_a} \left\{ m I_m \left(\frac{\chi'_{mn}\rho}{\rho_b} \right) (J_{m-1}(\rho\tau_{m'n'}) + J_{m+1}(\rho\tau_{m'n'})) \right. \\ &\left. + \frac{\chi'_{mn}\rho}{\rho_b} I'_m \left(\frac{\chi'_{mn}\rho}{\rho_b} \right) (J_{m-1}(\rho\tau_{m'n'}) - J_{m+1}(\rho\tau_{m'n'})) \right\} d\rho, \end{aligned}$$

which can be simplified with help of 9.1.27 in [1] to

$$\begin{aligned} \mathbf{E}_{1mn1}^T * \mathbf{R}_{1m'n'} &= -\frac{2\pi}{\sqrt{A_S}} \cos(m\varphi_{m'n'}) (-i)^{m-1} \\ &\times \int_{\rho_b}^{\rho_a} \left\{ \frac{m^2}{\rho\tau_{m'n'}} I_m \left(\frac{\chi'_{mn}\rho}{\rho_b} \right) J_m(\rho\tau_{m'n'}) + \frac{\chi'_{mn}\rho}{\rho_b} I'_m \left(\frac{\chi'_{mn}\rho}{\rho_b} \right) J'_m(\rho\tau_{m'n'}) \right\} d\rho. \end{aligned}$$

This expression can be simplified to

$$\begin{aligned} \mathbf{E}_{1mn1}^T * \mathbf{R}_{1m'n'} &= -\frac{2\pi}{\sqrt{A_S}} (\chi'_{mn})^2 \rho_b (-i)^{m-1} \cos(m\varphi_{m'n'}) \\ &\times \frac{I_m(\chi'_{mn}) J'_m(\rho_b \tau_{m'n'}) - c I_m(c \chi'_{mn}) J'_m(\rho_a \tau_{m'n'})}{\rho_b^2 \tau_{m'n'}^2 - (\chi'_{mn})^2}. \end{aligned}$$

Further it yields that

$$\mathbf{E}_{1mn2}^T * \mathbf{R}_{1m'n'} = \tan(m\varphi_{m'n'}) \mathbf{E}_{1mn1}^T * \mathbf{R}_{1m'n'}.$$

We now consider the convolution between the TE mode \mathbf{E}_{1mn1}^T and the Floquet wave $\mathbf{R}_{2m'n'}$. We use the same technique as before to get

$$\begin{aligned} \mathbf{E}_{1mn1}^T * \mathbf{R}_{2m'n'} &= \frac{1}{\sqrt{A_S}} \int_{\rho_b}^{\rho_a} d\rho \int_0^{2\pi} d\phi \left\{ m I_m \left(\frac{\chi'_{mn}\rho}{\rho_b} \right) \sin(m\phi) \cos(\phi - \varphi_{m'n'}) \right. \\ &\left. - \frac{\chi'_{mn}\rho}{\rho_b} I'_m \left(\frac{\chi'_{mn}\rho}{\rho_b} \right) \cos(m\phi) \sin(\phi - \varphi_{m'n'}) \right\} e^{-i\rho\tau_{m'n'} \cos(\phi - \varphi_{m'n'})}. \end{aligned}$$

We do the variable substitution $\phi - \varphi_{m'n'} \rightarrow \phi$ and obtain

$$\begin{aligned} \mathbf{E}_{1mn1}^T * \mathbf{R}_{2m'n'} &= \frac{1}{\sqrt{A_S}} \int_{\rho_b}^{\rho_a} d\rho \int_{-\varphi_{m'n'}}^{2\pi - \varphi_{m'n'}} d\phi \\ &\times \left\{ m I_m \left(\frac{\chi'_{mn}\rho}{\rho_b} \right) \sin(m(\phi + \varphi_{m'n'})) \cos \phi \right. \\ &\left. - \frac{\chi'_{mn}\rho}{\rho_b} I'_m \left(\frac{\chi'_{mn}\rho}{\rho_b} \right) \cos(m(\phi + \varphi_{m'n'})) \sin \phi \right\} e^{-i\rho\tau_{m'n'} \cos \phi}. \end{aligned}$$

As before we use the relations in (B.1) and note that the ϕ -integral with odd integrand is zero. We have

$$\begin{aligned} \mathbf{E}_{1mn1}^T * \mathbf{R}_{2m'n'} &= \frac{1}{\sqrt{A_S}} \sin(m\varphi_{m'n'}) \int_{\rho_b}^{\rho_a} d\rho \int_0^{2\pi} d\phi \left\{ m I_m\left(\frac{\chi'_{mn}\rho}{\rho_b}\right) \right. \\ &\times \left. \cos(m\phi) \cos\phi + \frac{\chi'_{mn}\rho}{\rho_b} I'_m\left(\frac{\chi'_{mn}\rho}{\rho_b}\right) \sin(m\phi) \sin\phi \right\} e^{-i\rho\tau_{m'n'} \cos\phi}, \end{aligned}$$

where we have changed the interval of integration to $0 \leq \phi \leq 2\pi$. As before we apply (B.2) and use that the integrand is even as function of ϕ around $\phi = \pi$,

$$\begin{aligned} \mathbf{E}_{1mn1}^T * \mathbf{R}_{2m'n'} &= \frac{1}{\sqrt{A_S}} \sin(m\varphi_{m'n'}) \int_{\rho_b}^{\rho_a} d\rho \int_0^\pi d\phi \\ &\times \left\{ m I_m\left(\frac{\chi'_{mn}\rho}{\rho_b}\right) (\cos((m-1)\phi) + \cos((m+1)\phi)) \right. \\ &\left. + \frac{\chi'_{mn}\rho}{\rho_b} I'_m\left(\frac{\chi'_{mn}\rho}{\rho_b}\right) (\cos((m-1)\phi) - \cos((m+1)\phi)) \right\} e^{-i\rho\tau_{m'n'} \cos\phi}. \end{aligned}$$

We perform the integration over ϕ and get

$$\begin{aligned} \mathbf{E}_{1mn1}^T * \mathbf{R}_{2m'n'} &= \frac{\pi}{\sqrt{A_S}} \sin(m\varphi_{m'n'}) (-i)^{m-1} \\ &\times \int_{\rho_b}^{\rho_a} \left\{ m I_m\left(\frac{\chi'_{mn}\rho}{\rho_b}\right) (J_{m-1}(\rho\tau_{m'n'}) - J_{m+1}(\rho\tau_{m'n'})) \right. \\ &\left. + \frac{\chi'_{mn}\rho}{\rho_b} I'_m\left(\frac{\chi'_{mn}\rho}{\rho_b}\right) (J_{m-1}(\rho\tau_{m'n'}) + J_{m+1}(\rho\tau_{m'n'})) \right\} d\rho. \end{aligned}$$

With the help of 9.1.27 in [1] this can be simplified to

$$\begin{aligned} \mathbf{E}_{1mn1}^T * \mathbf{R}_{2m'n'} &= \frac{2\pi}{\sqrt{A_S}} \sin(m\varphi_{m'n'}) m (-i)^{m-1} \\ &\times \int_{\rho_b}^{\rho_a} \left\{ I_m\left(\frac{\chi'_{mn}\rho}{\rho_b}\right) J'_m(\rho\tau_{m'n'}) + \frac{\chi'_{mn}}{\tau_{m'n'}\rho_b} I'_m\left(\frac{\chi'_{mn}\rho}{\rho_b}\right) J_m(\rho\tau_{m'n'}) \right\} d\rho. \end{aligned}$$

We now observe that the integrand can be written as

$$\frac{1}{\tau_{m'n'}} \frac{\partial}{\partial \rho} \left\{ I_m\left(\frac{\chi'_{mn}\rho}{\rho_b}\right) J_m(\rho\tau_{m'n'}) \right\}$$

and the remaining integration is easy to do. We get

$$\begin{aligned} \mathbf{E}_{1mn1}^T * \mathbf{R}_{2m'n'} &= \frac{2\pi}{\sqrt{A_S}} \sin(m\varphi_{m'n'}) m (-i)^{m-1} \\ &\times \frac{I_m(c\chi'_{mn}) J_m(\rho_a\tau_{m'n'}) - I_m(\chi'_{mn}) J_m(\rho_b\tau_{m'n'})}{\tau_{m'n'}}. \end{aligned}$$

Further it yields that

$$\mathbf{E}_{1mn2}^T * \mathbf{R}_{2m'n'} = -\cot(m\varphi_{m'n'}) \mathbf{E}_{1mn1}^T * \mathbf{R}_{2m'n'}.$$

B.1.3 TM modes

Next we study the convolution between the TM mode \mathbf{E}_{2mn1}^T and the Floquet wave $\mathbf{R}_{2m'n'}$. We have

$$\begin{aligned} \mathbf{E}_{2mn1}^T * \mathbf{R}_{2m'n'} &= \frac{1}{\sqrt{A_S}} \int_{\rho_b}^{\rho_a} d\rho \int_0^{2\pi} d\phi \left\{ m Z_m\left(\frac{\chi_{mn}\rho}{\rho_b}\right) \cos(m\phi) \sin(\phi - \varphi_{m'n'}) \right. \\ &\quad \left. - \frac{\chi_{mn}\rho}{\rho_b} Z'_m\left(\frac{\chi_{mn}\rho}{\rho_b}\right) \sin(m\phi) \cos(\phi - \varphi_{m'n'}) \right\} e^{-i\rho\tau_{m'n'} \cos(\phi - \varphi_{m'n'})}. \end{aligned}$$

The variable substitution $\phi - \varphi_{m'n'} \rightarrow \phi$ gives

$$\begin{aligned} \mathbf{E}_{2mn1}^T * \mathbf{R}_{2m'n'} &= \frac{1}{\sqrt{A_S}} \int_{\rho_b}^{\rho_a} d\rho \int_{-\varphi_{m'n'}}^{2\pi - \varphi_{m'n'}} d\phi \\ &\quad \times \left\{ m Z_m\left(\frac{\chi_{mn}\rho}{\rho_b}\right) \cos(m(\phi + \varphi_{m'n'})) \sin \phi \right. \\ &\quad \left. - \frac{\chi_{mn}\rho}{\rho_b} Z'_m\left(\frac{\chi_{mn}\rho}{\rho_b}\right) \sin(m(\phi + \varphi_{m'n'})) \cos \phi \right\} e^{-i\rho\tau_{m'n'} \cos \phi}, \end{aligned}$$

which can be simplified with the help of (B.1) to

$$\begin{aligned} \mathbf{E}_{2mn1}^T * \mathbf{R}_{2m'n'} &= -\frac{1}{\sqrt{A_S}} \sin(m\varphi_{m'n'}) \int_{\rho_b}^{\rho_a} d\rho \int_0^{2\pi} d\phi \left\{ m Z_m\left(\frac{\chi_{mn}\rho}{\rho_b}\right) \right. \\ &\quad \left. \times \sin(m\phi) \sin \phi + \frac{\chi_{mn}\rho}{\rho_b} Z'_m\left(\frac{\chi_{mn}\rho}{\rho_b}\right) \cos(m\phi) \cos \phi \right\} e^{-i\rho\tau_{m'n'} \cos \phi}, \end{aligned}$$

where we have used that the ϕ -integrals with odd integrands are zero. Further we use (B.2) and get

$$\begin{aligned} \mathbf{E}_{2mn1}^T * \mathbf{R}_{2m'n'} &= -\frac{1}{\sqrt{A_S}} \sin(m\varphi_{m'n'}) \int_{\rho_b}^{\rho_a} d\rho \int_0^\pi d\phi \\ &\quad \times \left\{ m Z_m\left(\frac{\chi_{mn}\rho}{\rho_b}\right) (\cos((m-1)\phi) - \cos((m+1)\phi)) \right. \\ &\quad \left. + \frac{\chi_{mn}\rho}{\rho_b} Z'_m\left(\frac{\chi_{mn}\rho}{\rho_b}\right) (\cos((m-1)\phi) + \cos((m+1)\phi)) \right\} e^{-i\rho\tau_{m'n'} \cos \phi}. \end{aligned}$$

With the help of 9.1.21 in [1] we can carry out the integration over ϕ . We get that

$$\begin{aligned} \mathbf{E}_{2mn1}^T * \mathbf{R}_{2m'n'} &= -\frac{\pi}{\sqrt{A_S}} \sin(m\varphi_{m'n'}) (-i)^{m-1} \\ &\quad \times \int_{\rho_b}^{\rho_a} \left\{ m Z_m\left(\frac{\chi_{mn}\rho}{\rho_b}\right) (J_{m-1}(\rho\tau_{m'n'}) + J_{m+1}(\rho\tau_{m'n'})) \right. \\ &\quad \left. + \frac{\chi_{mn}\rho}{\rho_b} Z'_m\left(\frac{\chi_{mn}\rho}{\rho_b}\right) (J_{m-1}(\rho\tau_{m'n'}) - J_{m+1}(\rho\tau_{m'n'})) \right\} d\rho, \end{aligned}$$

which can be simplified, with the help of 9.1.27 in [1], to

$$\mathbf{E}_{2mn1}^T * \mathbf{R}_{2m'n'} = -\frac{2\pi}{\sqrt{A_S}} \sin(m\varphi_{m'n'}) (-i)^{m-1} \\ \times \int_{\rho_b}^{\rho_a} \left\{ \frac{m^2}{\rho\tau_{m'n'}} Z_m\left(\frac{\chi_{mn}\rho}{\rho_b}\right) J_m(\rho\tau_{m'n'}) + \frac{\chi_{mn}\rho}{\rho_b} Z'_m\left(\frac{\chi_{mn}\rho}{\rho_b}\right) J'_m(\rho\tau_{m'n'}) \right\} d\rho.$$

This expression can be simplified to

$$\mathbf{E}_{2mn1}^T * \mathbf{R}_{2m'n'} = -\frac{2\pi}{\sqrt{A_S}} \chi_{mn}\rho_b (-i)^{m-1} \sin(m\varphi_{m'n'}) \rho_b \tau_{m'n'} \\ \times \frac{cZ'_m(c\chi_{mn}) J_m(\rho_a \tau_{m'n'}) - Z'_m(\chi_{mn}) J_m(\rho_b \tau_{m'n'})}{\rho_b^2 \tau_{m'n'}^2 - \chi_{mn}^2}.$$

In conclusion it yields that

$$\mathbf{E}_{2mn2}^T * \mathbf{R}_{2m'n'} = \cot(m\varphi_{m'n'}) \mathbf{E}_{2mn1}^T * \mathbf{R}_{2m'n'}.$$

References

- [1] M. Abramowitz and I. A. Stegun, editors. *Handbook of Mathematical Functions*. Applied Mathematics Series No. 55. National Bureau of Standards, Washington D.C., 1970.
- [2] R. E. Collin. *Field Theory of Guided Waves*. IEEE Press, New York, second edition, 1991.
- [3] Computer Solutions Europe AB, Stockholm. *FEMLAB: Reference Manual*, 1998.
- [4] J. D. Jackson. *Classical Electrodynamics*. John Wiley & Sons, New York, third edition, 1999.
- [5] N. Marcuvitz. *Waveguide handbook*. McGraw-Hill, New York, 1951.
- [6] G. Pelosi, R. Coccioli, and S. Selleri. *Quick Finite Elements for Electromagnetic Waves*. Artech House, London, 1998.
- [7] R. Petit, editor. *Electromagnetic Theory of Gratings*, volume 22 of *Topics in Current Physics*. Springer-Verlag, Heidelberg, 1980.
- [8] A. Roberts. *Modal methods for gratings, grids and apertures*. PhD thesis, School of Physics, University of Sydney, 1988.

- [9] A. Roberts and R. C. McPhedran. Bandpass grids with annular apertures. *SPIE Application and Theory of Periodic Structures, Diffraction Gratings, and Moire Phenomena*, **815**(3), 73–78, 1987.
- [10] A. Roberts and R. C. McPhedran. Bandpass grids with annular apertures. *IEEE Trans. on Antennas and Propagation*, **36**(5), 607–611, May 1988.
- [11] A. Roberts, M. L. von Bibra, H.-P. Gemünd, and E. Kreysa. Thick grids with circular apertures: a comparison of theoretical and experimental performance. *International Journal of Infrared and Millimeter Waves*, **15**(3), 505–517, 1994.
- [12] C.-H. Tsao and R. Mittra. Spectral-domain analysis of frequency selective surfaces comprised of periodic arrays of cross dipoles and Jerusalem crosses. *IEEE Trans. Antennas Propagat.*, **32**(5), 478–486, 1984.
- [13] T. K. Wu, editor. *Frequency Selective Surface and Grid Array*. John Wiley & Sons, New York, 1995.